

# C 2    **Hydrodynamics**

Walter Zimmermann

Theoretische Physik I

Universität Bayreuth

## **Contents**

<b>1</b>	<b>Introduction</b>	<b>2</b>
<b>2</b>	<b>Fluid dynamics of Newtonian Fluids</b>	<b>6</b>
2.1	Thermal convection . . . . .	6
2.2	Nonlinear properties beyond the onset of convection . . . . .	9
<b>3</b>	<b>Flow at low values of the Reynolds number <math>Re</math></b>	<b>11</b>
3.1	Dimensionless Navier-Stokes equation and the Reynolds number . . . . .	11
3.2	Example: Plane Poiseuille Flow . . . . .	12
3.3	Particles in a Newtonian fluid . . . . .	12
3.4	Effect of a dilute suspension of particles on the shear viscosity . . . . .	16
3.5	Elastic turbulence in polymeric solutions at small $Re$ . . . . .	17
<b>4</b>	<b>Nematic liquid crystals</b>	<b>18</b>
<b>5</b>	<b>Polymer liquids</b>	<b>22</b>
5.1	Linear Viscoelasticity - Maxwell Model . . . . .	22
5.2	Nonlinear deformations of viscoelastic fluids . . . . .	23
5.3	Example: Pipeflow for a shear thinning fluid . . . . .	24
<b>A</b>	<b>Equations of motion for Newtonian fluids</b>	<b>26</b>
<b>B</b>	<b>Derivation of the Oseen-Tensor</b>	<b>30</b>

# 1 Introduction

Various types of flows are among our everyday experience. There are flows (winds) in the atmosphere, flows of water or oil through pipes, flows around air plane wings, in rivers, blood flow through our veins and arteries, fluid motion during cooking etc.. Motion counts to the most fascinating states of matter and flows exhibit a great variety of motion and of nonlinear phenomena. With the Navier-Stokes equation (NSE) there is a theoretical framework available for simple (Newtonian) fluids like water, olive oil etc. that is known already since the 19th century [1, 2]. Due to the inherent nonlinear character of many flows it is hard to obtain analytical solutions of the NSE or of the NSE coupled to the heat conducting equation. However, numerical methods combined with computer power, sophisticated computer assisted experiments and new concepts from chaos theory and pattern formation have provided important new insights about various kinds of Newtonian flows during the last two decades. For viscoelastic liquids the basic equations are much less established and in this field one needs besides smart computer codes also theoretical progress for establishing appropriate equations of motion.

- Classical fluid dynamics with its huge variety in flow problems in engineering, in geophysics and meteorology belongs to the huge field of hydrodynamics. Many efforts in these areas are directed towards an improved understanding of **turbulent fluid motion** for practical purposes and they rely very often on a statistical analysis. The transition scenarios to turbulence are not known for all types of flows. For instance, a novel bifurcation scenario has been identified in pipe flow quite recently [3, 4].

Thermal convection was first studied by Henri Bénard (1874-1939) more than hundred years ago and explained by Lord Rayleigh. An overview about a number of recent and surprising insights about turbulence in that system may be found in [5] and the references therein.

- Many investigations about various kinds of **bifurcation scenarios in chaos and pattern formation**, another huge area of activities, have its starting point in hydrodynamics. Fluid dynamicists are well aware of so-called coherent structures that are observed in turbulent fluid motions, and often these structures can be related to instabilities of a basic laminar state, such as in Rayleigh-Bénard convection or in Taylor-Vortex-Flow (see Fig. 1).

In Taylor-Vortex flow the control parameter is for instance the rotational frequency of the inner cylinder. In Rayleigh-Bénard convection it is the temperature difference between the upper and lower boundary. In an extended layer of Rayleigh-Bénard convection one has in the center of the cell essentially rotational invariance. This rotational invariance is broken for an inclined convection layer and the inclination angle provides an additional control parameter. A horizontal flux through a Rayleigh-Bénard cell breaks also the rotational symmetry in the  $x - y$  plane. With such a symmetry breaking one can mimic winds in convection layers in the atmosphere. Other examples with a broken rotational symmetry are convection experiments with nematic liquid crystals, another field with fascinating flow patterns [7, 8].

In thermal convection many fundamental phenomena have been observed for the first time. The occurrence of chaos goes back to a three mode model of Lorenz [9], derived from the fundamental equations of thermal convection. Period doubling phenomena on the route to chaos have been observed in thermal convection [10]. Recently in this well known system spiral defect chaos has been discovered [11] and even in turbulence new

## Examples

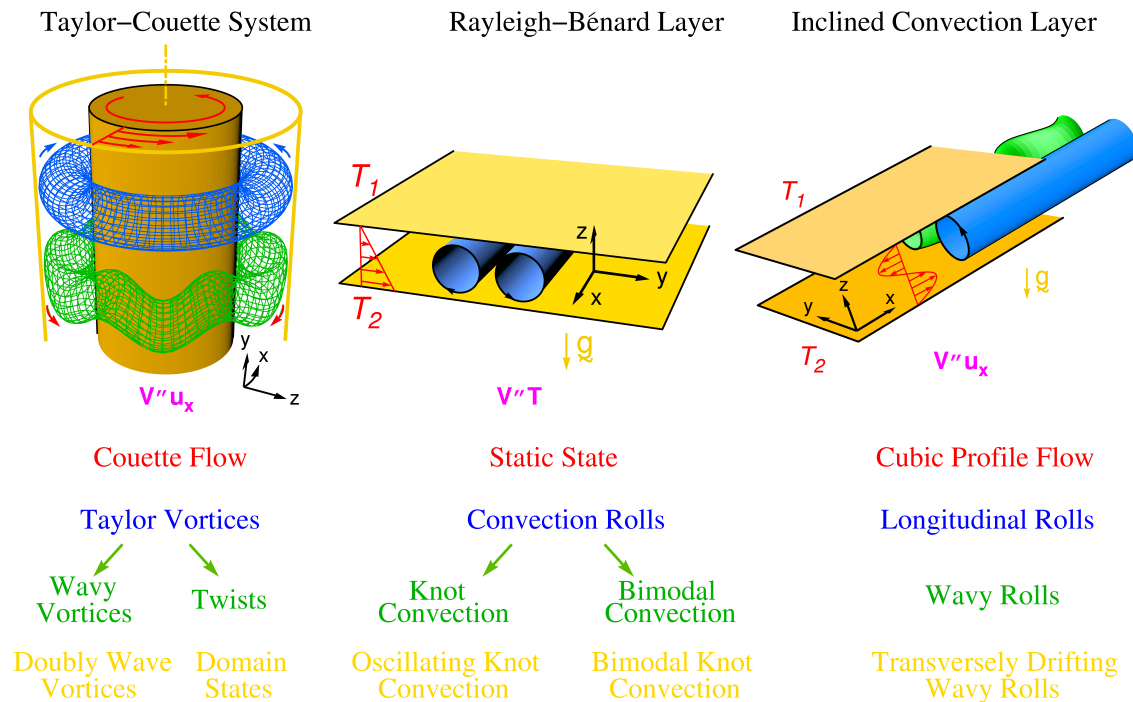


**Fig. 1:** Paradigmatic flow systems to investigate with increasing external stress (increasing values of the control parameter) sequences of bifurcations experimentally and by advanced computational methods [6].

phenomena have been observed quite recently [5]. Many other investigations on thermal convection and other pattern forming systems are summarized in the review of Cross and Hohenberg [12].

- **Microfluidics** is another and expanding branch of hydrodynamics [13]. This research area is restricted to flows through narrow channels and therefore to low Reynolds number hydrodynamics. But the flows here are often strongly influenced by suspended particles such as polymers, red blood cells etc. .
- **Flow problems in complex fluids.** Complex fluids exhibit a great variety of fluid phases and ordering phenomena in thermal equilibrium. The origin of these different phases are competing interactions in these materials.

Liquid crystals are examples of fluids with an internal, spontaneously broken symmetry. Especially nematic liquid crystals are nearly omnipresent nowadays due to their applications in liquid crystal displays (**LCD**). Liquid crystals are switched by an applied voltage. In a quite similar configuration electrohydrodynamic instabilities and bifurcations occur, where an additional coupling between the flow field and the nematic ordering takes place. This leads to a number of fascinating patterns as shown for instance in Fig. 2. Much more images of similar flow patterns (discovered and partially explained quite recently) may be found in Refs. [7, 8, 14, 15, 16, 17, 12].

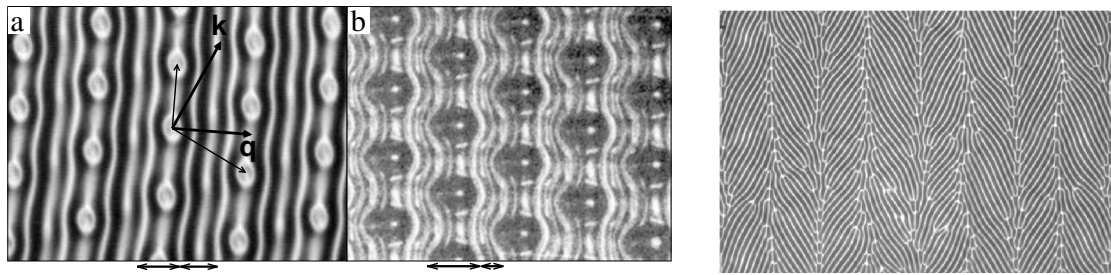


**Fig. 2:** *These are images of flow patterns occurring in electrically driven nematic liquid crystals. These patterns are observed in an experimental configuration which is rather similar to that of a liquid crystal display (LCD), a device which is used in many applications today. In nematic liquid crystals the viscosity is anisotropic. Nematics have also elastic properties and their interplay with flow leads to the numerous fascinating patterns in these materials, more of them may be found in Refs. [14, 7, 8, 15, 16]. The pattern shown in the left part has been understood only recently [18].*

Suspended particles change the shear viscosity. Einstein calculated in 1906 this effect and obtained in the diluted regime without interactions between particles, that the shear viscosity increases with the density of the particles [19]. If the particles are deformable such as vesicles then the shear viscosity is less increased as shown recently [20].

Suspensions often lead to a nonlinear relationship between the flow rate of a laminar flow through a pipe and the pressure drop. In such a case the shear viscosity depends on the shear rate itself, a typical signature of non-Newtonian fluids. The majority of complex fluids are shear thinning, i.e. their viscosities decrease with the shear-rate. A few fluids are also shear thickening. The shear thinning occurs for instance by deformations of suspensions.

Polymers in solution may be considered as deformable suspensions. Undeformable suspensions are less related to elastic and memory effects than suspended polymers. Elastic effects change the time-dependence of flows enormously. Another effect are normal stresses which play a role for instance in rod climbing of viscoelastic fluids, the so-called Weissenberg effect.

In ferrofluids one has suspended particles that carry a magnetic moment. The flow properties may depend on dipole-dipole interaction and viscosity may be varied by the strength of an applied magnetic field. More about ferrofluids may be found in [21, 22, 23]. In a similar manner the viscosity in an electrorheological fluid, (where the particles carry an electric dipole) can be varied over a wide range by application of an electrical field [24].

- **Polymeric fluids - viscoelastic fluids.** The entropic elasticity of polymers leads to very fascinating phenomena in polymer solutions. Prominent and astonishing examples are the Weissenberg effect (rod climbing effect) and the turbulent drag reduction as shown in Fig. 3.

Only a few ppm of polyethylene oxide added to water reduce the effective viscosity in a fire hose by a huge amount. As a consequence, a jet of pure water leaves the fire hose much slower but under the same conditions, the same pumping power, the same fire hoses,

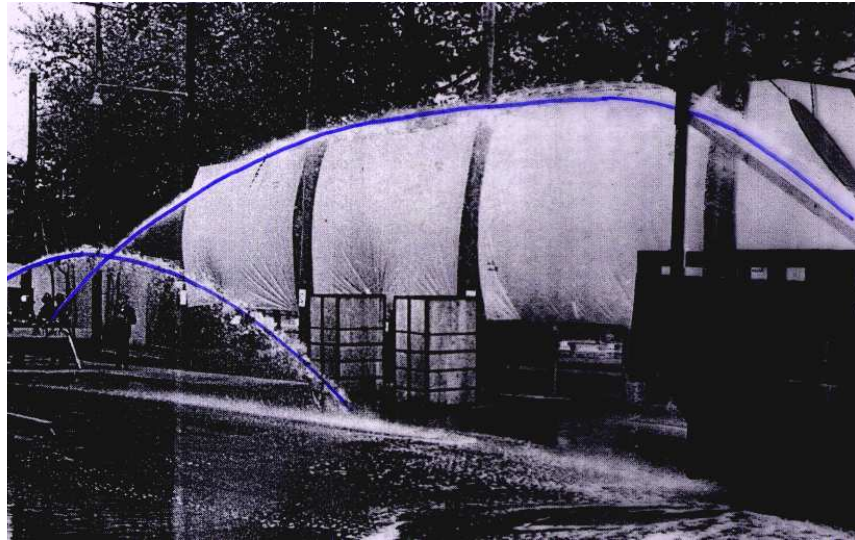


**Fig. 3:** *Demonstration of turbulent drag reduction with two fire hoses as an example for flow phenomena in viscoelastic fluids. Through one fire hose (the left one) pure water is pumped and through the other one water containing 0.003% polyethylene oxide (from Bailey & Koleske: Poly(Ethylene Oxide), Academic Press 1976).*

the same inclination angle etc. than the jet of water including a few ppm poly-(ethylene) oxide. The mean velocity of turbulent flows through pipes may be enhanced by polymer additives up to a factor of ten. This effect of turbulent drag reduction is also used in the Trans Alaskan oil pipelines in order to save pumping power and in a Bristol sewer pipe. There are suggestions for explanations of this phenomenon, but a number of questions are left open and this problem is still a matter of current research. However, it seems rather obvious that the entropic elasticity of polymers plays a crucial role for this phenomenon. Further examples of viscoelastic flow effects may be found in volume I of Bird et al. [26].

Polymer liquids are not only fascinating in flows at large Reynolds numbers. The deformability of polymers and their entropic elasticity leads even in flows at low Reynolds numbers to turbulent flow behavior, the so-called elastic turbulence [29]. This behavior may be also used in microfluidics for mixing substances [30]. A theoretical foundation of this effect is still missing too.

- Hydrodynamics in general is a method to describe macroscopic states of matter by fields that are continuously varying in space and time. It covers the long wavelength dynamics. The concepts of hydrodynamics used for the previously mentioned examples are at present further developed and applied even to continuum aspects of the dynamics of the skeleton of biological cells. This is a rather new direction with very interesting perspectives. These and further recent developments in soft matter physics may be summarized also under the notion **Nonlinear Dynamics of Complex Continua** (<http://www.for608.uni-bayreuth.de>).

## 2 Fluid dynamics of Newtonian Fluids

The derivation of the equations of motion of simple fluids is based on mass, energy and momentum conservation, simple linear transport laws for the heat and the second law of thermodynamics. A detailed derivation of the basic equations may be found in many textbooks. A rather complete description is given for instance in volume VI of the textbook series of Landau-Lifshitz [1]. A more generalized point of view may be found in the book of Chaikin/Lubensky [31]. Further introductory texts on classical fluids are Tritton [32] and Acheson [2].

The dynamics of a Newtonian fluid is described by a velocity field  $\mathbf{u}(\mathbf{r}, t)$ , by the mass density  $\rho$  (the time and spatial dependence is only considered in this section in front of the gravitational force  $\mathbf{g}$ ), the temperature field  $T(\mathbf{r}, t)$  and the pressure field  $p(\mathbf{r}, t)$ . The equations of motion are given by (see also appendix A)

$$\rho \partial_t \mathbf{u} + \rho (\mathbf{u} \cdot \nabla) \mathbf{u} = -\nabla p + \rho \mathbf{g} + \eta \nabla^2 \mathbf{u} \quad , \quad (1)$$

$$\partial_t T + (\mathbf{u} \cdot \nabla) T = \kappa \Delta T \quad . \quad (2)$$

### 2.1 Thermal convection

Rayleigh-Bénard convection is one of the most investigated fluid dynamics systems [33, 34, 35, 36, 37]. Convection patterns have been observed by H. Bénard [33, 34] nearly 100 years ago and a first theory was provided by Lord Rayleigh nearly 90 years ago [38, 39]. By cooking liquids everybody can observe thermal convection.

This system exhibits still new phenomena and is especially used for investigations of generic nonlinear phenomena, that occur very likely in many other systems, such as chaos [40, 12] and various stationary as well as spatiotemporal patterns [37, 12].

In addition this system allows the determination of the transition from thermal conduction to convection by an elementary calculation. The mechanism for the onset of convection can be found in many different places as for instance in Ref. [5].

Thermal convection is usually investigated between two parallel plates in a gravitational field as indicated by Fig. 4. Convection sets in, when the temperature difference  $\Delta T$  increases beyond a critical value that depends on the layer height, the viscosity of the fluid etc. (see below).

Below the onset of convection the  $z$ -dependent heat is transported by heat conduction without convection and the solution of Eq. (2) is in this case described by

$$T(z) = \Delta T(1 - z/d) + T_1 \quad . \quad (3)$$

We call this linear temperature profile without convection the basic state, which is translationally invariant with respect to  $x$  and  $y$  in the plane of the convection layer, if we assume an infinitely extended fluid layer.

By thermal extension the lighter fluid is at the bottom, which corresponds to an inherently unstable state in the gravitational field. This unstable state persists up to a critical temperature difference, which we calculate in this section.

A rescaling of the two equations, as described in appendix A, leads to the introduction of two dimensionless variables, the Rayleigh number  $R$  and the Prandtl number  $P$ :

$$R = \frac{\rho_0 \alpha g \Delta T d^3}{\kappa \nu} \quad , \quad P = \frac{\nu}{\kappa} \quad . \quad (4)$$

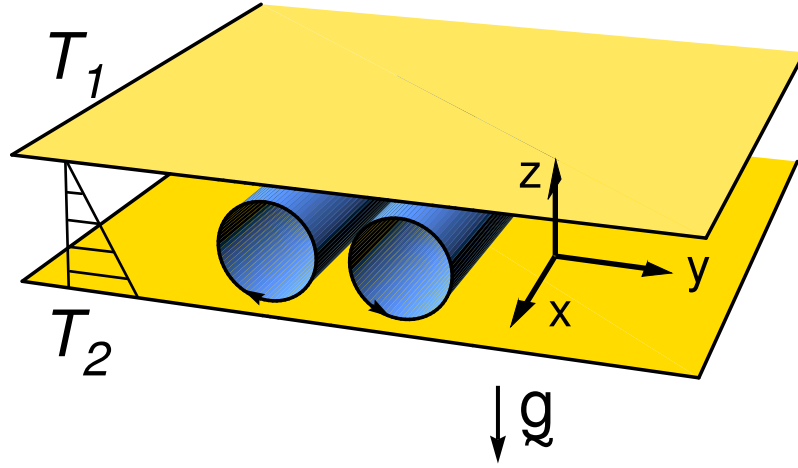


**Fig. 4:** A schematic drawing of a Rayleigh-Bénard convection cell with the layer height  $d$ , where the heat current  $Q$  is transported through the cell according to the temperature difference  $\Delta T = T_2 - T_1$  between the temperature at the bottom  $T_2$  and the temperature  $T_1$  at the top boundary.

$P$  is the ratio between kinematic viscosity  $\nu = \eta/\rho_0$  and the thermal diffusivity  $\kappa$ .  $R$  is the control parameter of the system and it is the dimensionless ratio between the buoyancy force  $\rho_0 \alpha g \Delta T d^3$  and the product of the friction  $\nu$  and the thermal diffusivity  $\kappa$ .  $\alpha$  is the thermal expansion coefficient and  $d$  is the layer height.

**Determination of the onset of thermal convection.** Here we determine the critical value of  $R$  at which the basic heat conducting fluid becomes unstable and convection sets in. For this we use the equations of motion for the velocity potential  $\Psi$  and the temperature  $T$  in Boussinesq approximation, but restricted to two spatial dimensions, as derived in appendix A. The velocity potential  $\Psi$  and the velocity components are related as follows  $\vec{v} = (v_y, 0, v_z) = (\partial_z \Psi, 0, -\partial_y \Psi)$ . Since one has in an infinitely extended fluid rotational invariance, i.e. the orientation of the convection rolls is arbitrary, a stability calculation for two spatial dimensions is sufficient. The deviation from the linear temperature profile we denote by  $\Theta$ .

$$\begin{aligned} \frac{1}{P} \partial_t \Delta \Psi + \partial_y \Theta - \Delta^2 \Psi &= \frac{1}{P} (\partial_z \Psi \partial_y - \partial_y \Psi \partial_z) \Delta \Psi, \\ \partial_t \Theta - \Delta \Theta + R \partial_y \Psi &= -(\partial_z \Psi \partial_y - \partial_y \Psi \partial_z) \Theta. \end{aligned} \quad (5)$$

Since  $\Theta$  and  $\Psi$  describe the deviations from the basic state, it is sufficient to investigate the growth properties of small perturbations in  $\Theta$  and  $\Psi$ . This procedure is the so-called stability analysis and for that we can neglect products of both fields in the equations.

The linear part of the two coupled equations (5) are partial differential equations with constant coefficients and such a type of equations is solved by a Fourier ansatz. In  $y$ -direction we assume periodic boundary conditions to the infinite extension. If we assume for simplicity free slip boundary conditions for the horizontal components of the velocity, as described in appendix A, we can solve the linear part of Eqs. (5) with an analytical ansatz as follows

$$\begin{aligned} \Theta(t, y, z) &= \bar{\Theta} e^{\sigma t} \cos(\pi z) \cos(ky), \\ \Psi(t, y, z) &= \bar{\Psi} e^{\sigma t} \cos(\pi z) \sin(ky). \end{aligned} \quad (6)$$

Here  $\bar{\Theta}$  and  $\bar{\Psi}$  are constant amplitudes. For  $\bar{\Theta}, \bar{\Psi} \neq 0$  the solubility condition for the resulting homogeneous equations in the amplitudes  $\bar{\Theta}$  and  $\bar{\Psi}$  provides the expression for the dispersion relation

$$\sigma_{1,2} = -(\pi^2 + k^2) \left(1 + \frac{1}{P}\right) \pm \sqrt{(\pi^2 + k^2)^2 \left[ \left(1 + \frac{1}{P}\right)^2 - 4 \right] + \frac{4k^2 R}{\pi^2 + k^2}}. \quad (7)$$

The first contribution to  $\sigma_{1,2}$  is always negative. Therefore the growth rate  $\text{Re}[\sigma_1]$  can become positive only if the expression under the square root is positive. Since this is always the case the basic state becomes only unstable with respect to non-oscillatory perturbations. For each wave number  $k$  the basic state becomes unstable for a different value of  $R$ . The *neutral stability condition*  $\text{Re}[\sigma] = 0$  separates the parameter range, where the basic state is unstable from that range where the basic state is stable. With the condition  $\text{Re}[\sigma] = 0$  one gets with

$$R_0(k) = \frac{(\pi^2 + k^2)^3}{k^2}, \quad (8)$$

the expression for the so-called neutral curve as shown in Fig.5a). Below this curve the homogeneous basic state is linearly stable and beyond unstable.

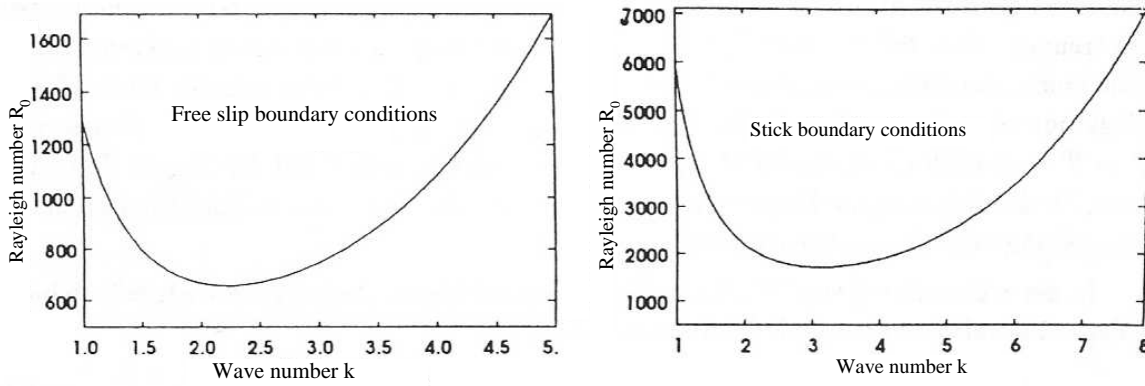


**Fig. 5:** a) The neutral curve  $R_0(k)$  for free slip boundary conditions defined by Eq. (87) and in b) for realistic boundary conditions as defined by Eq. (86).

Experimentally the wave number cannot be chosen. The thermal fluctuations include a broad spectrum of wave numbers and only those will be amplified with  $(R, k)$  beyond the neural curve. Hence the minimum of  $R_0(k)$  tells, at which temperature difference the basic state becomes unstable. The values at the minimum are

$$R_c = \frac{27}{4} \pi^4 \approx 657.51, \quad k_c = \frac{\pi}{\sqrt{2}} \approx 2.221 \quad (\text{free boundary}). \quad (9)$$

The great advantage of the used free slip boundary conditions is that the stability calculation could be done analytically. For realistic non slip boundary conditions one has to use appropriate numerical methods and the critical values are in this case

$$R_c = 1707.76... , \quad k_c = 3.116 \quad (\text{realistic boundary}). \quad (10)$$

The neutral curve for non slip boundary conditions is shown Fig. 5b). These critical values of dimensionless parameters are universal numbers. Whatever kind of Newtonian fluid is used, these numbers are always the same. However, the corresponding temperature difference changes with the material parameters of the substances, c.f. Eq. (4).



**The Eigenvector.** Since for the determination of the critical values we have solved an eigenvalue problem, the two amplitudes  $\bar{\Theta}$  and  $\bar{\Psi}$  are not independent. The linear solution at  $(R_c, k_c)$  is

$$\vec{u}_1 = \begin{pmatrix} \Psi \\ \Theta \end{pmatrix} = [A e^{ik_c y} + A^* e^{-ik_c y}] \vec{U}_1(z) \quad \text{with} \quad \vec{U}_1 = \begin{pmatrix} 4i/\pi \\ 9\sqrt{2}\pi^2 \end{pmatrix} \cos(\pi z). \quad (11)$$

For non slip boundary conditions  $\vec{U}_1(z)$  has to be determined numerically (see for two different methods either Ref. [35] or Ref. [41]). The amplitude  $A$  of the eigenfunction is the so-called order parameter because it is a measure for the strength of the new order beyond the instability. By introducing a small parameter  $\varepsilon = (R - R_c)/R_c$  and  $k - k_c$  one may cover the behavior in a small neighborhood of  $(R_c, k_c)$  by an equation for the amplitude  $A(y, t)$  where  $A(y, t)$  covers slow modulations of the spatially periodic structure and the slow dynamics [42, 12, 41],

$$\tau_0 \partial_t A = \varepsilon A + \xi_0^2 \partial_y^2 A - g|A|^2 A, \quad (12)$$

with

$$\tau_0 = \frac{1}{R_c \frac{\partial \sigma_1}{\partial R}} = \frac{2}{3\pi^2}, \quad \xi_0^2 = \frac{1}{2R_c} \frac{\partial^2 R}{\partial k^2} = \frac{8}{3\pi^2}, \quad (13)$$

for free slip boundary conditions. The nonlinear coefficient is positive for thermal convection and therefore the bifurcation is continuous, i.e. supercritical.

## 2.2 Nonlinear properties beyond the onset of convection

Close to the threshold in extended systems straight roll convection is observed. This is also what analytical and numerical solutions of the NSE imply. These straight roll solutions are stable for wave numbers in a subrange above the neutral curve in Fig. 5b), which is bounded by the Eckhaus stability boundary (right) and the Zig-Zag instability (left). There is excellent agreement between the observation of convection rolls and their theoretical description. The wave number range, where convection rolls are stable as a function of  $R, P$  and  $k$ , is the so-called Busse-balloon [6] (F. H. Busse is Professor at the University of Bayreuth).

If the convection cell has only finite extension in the  $x - y$  plane then convection rolls tend to stay with their axis perpendicular to the container boundaries as shown in Fig. 6. This can be predicted in terms of amplitude equations as given in Eq. (12), but extended to two dimensions [12, 43].

Rayleigh-Bénard convection has been studied for more than one century, but roughly one decade ago the researchers were very surprised by observing Spiral-Defect-Chaos. In a parameter range, where the convection rolls have been shown to be stable experimentally and by calculations, they found as a second nonlinear state the spatiotemporally complex state of Spiral-Defect-Chaos (SDC). Two snapshots of the dynamical state are given in Fig. 7. Characteristic for this state is the persistent creation and annihilation of spiral-defects.

By increasing the Rayleigh number  $R$  further beyond  $R_c$  a sequence of bifurcations and patterns may be found as indicated in Fig. 1. Turbulent convection takes place at much higher values of the Rayleigh number. Large values of the Rayleigh number  $R$  can be achieved in high containers with large values of  $d$ . In one experiment at the university of Illmenau  $d$  is several meters and the convection cell is a building. So the aspect ratio  $\Gamma$ , the ratio between the horizontal extension and  $d$ , is small, as for instance indicated in Fig. 8.

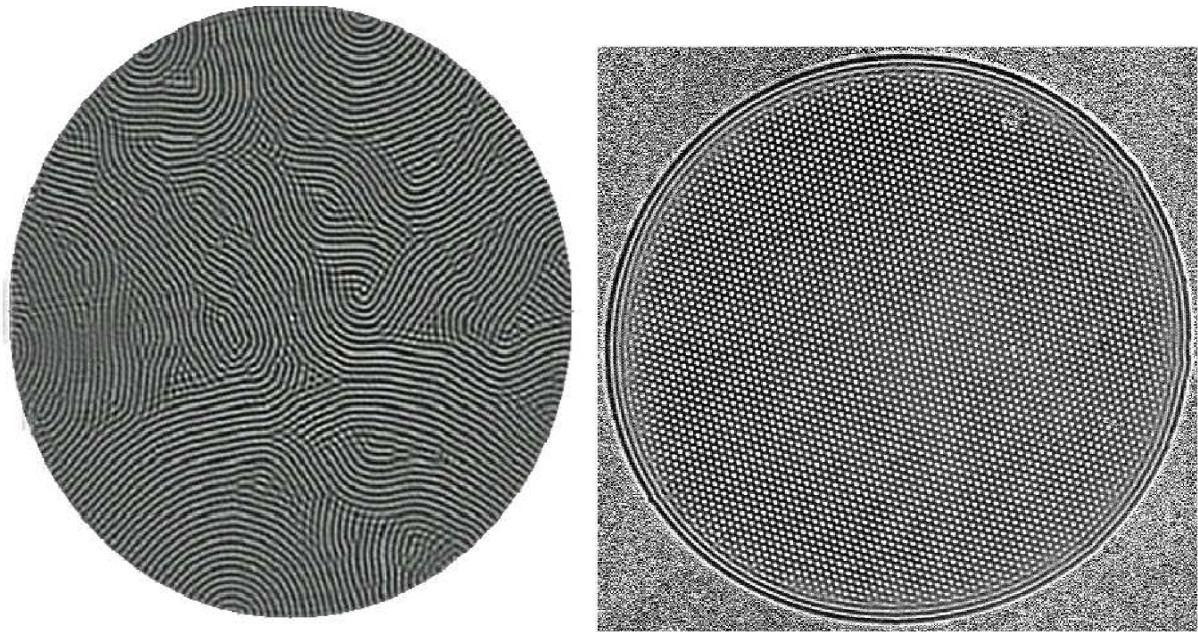


**Fig. 6:** a) Convection rolls in intrinsically isotropic systems, such as Rayleigh-Bénard convection, orient with their axis of rolls perpendicular to the side walls of the convection cell. b) In certain fluids, like water close to  $4^{\circ}\text{C}$ , close to the threshold hexagonal patterns occur.

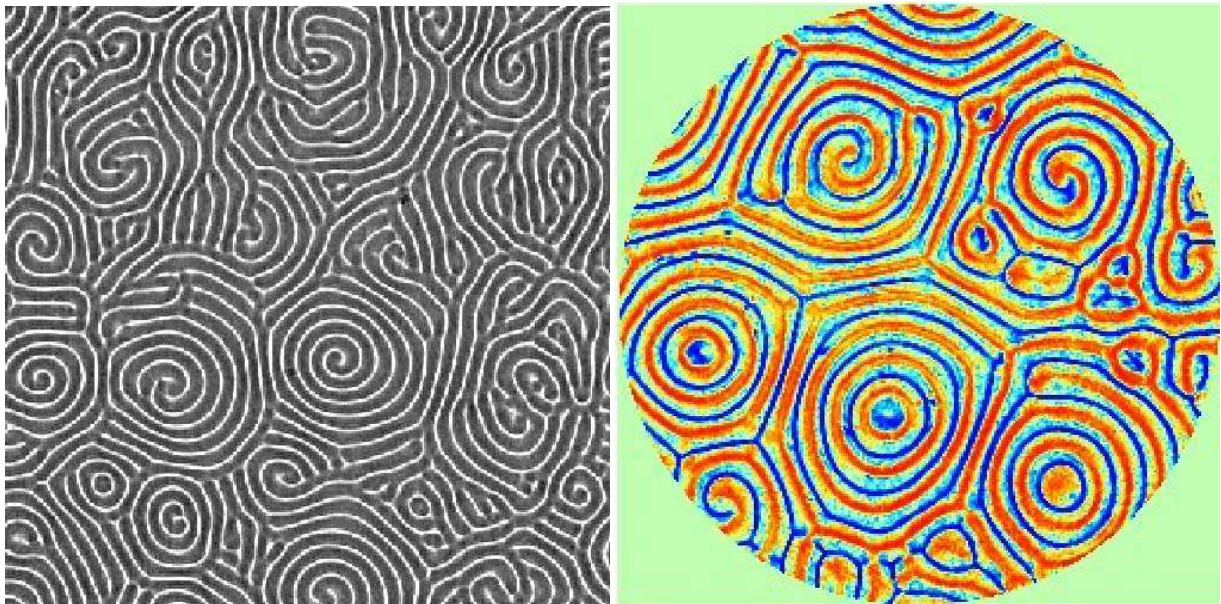


**Fig. 7:** In a range for the Rayleigh number  $R$  where straight rolls are still linearly stable only one decade ago the so-called Spiral-Defect-Chaos has been observed in experiments both in rectangular and circular convection cells (see [11] and references therein).

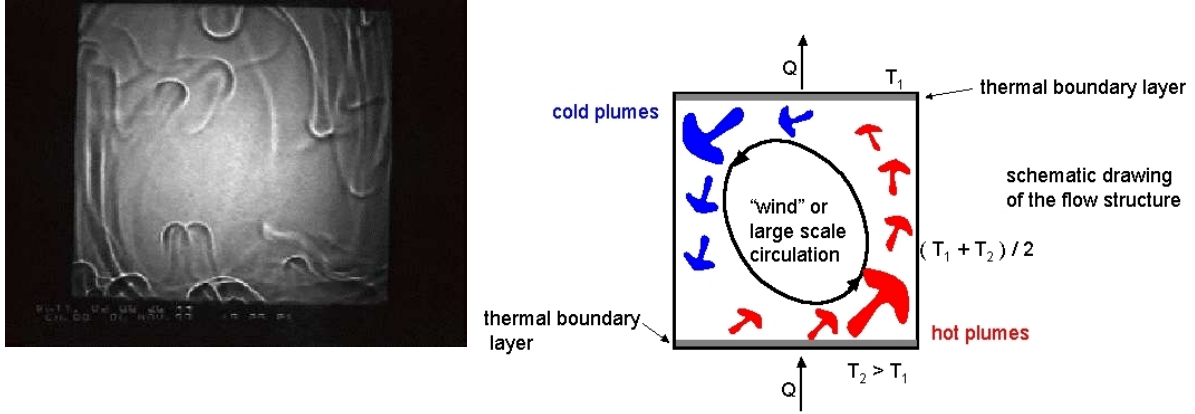


**Fig. 8:** A snapshot of turbulent convection at very large values of  $R = 6.8 \cdot 10^8$  and a small aspect ratio  $\Gamma = 1$  ( $P = 596$ ). The right part shows that there is a large scale motion (“Wind of turbulence”) superimposed with turbulent motion down to very small scales (see e.g. [5, 46]).

The influence of spatially varying boundary conditions on pattern formation (or more general heterogeneity effects) is another aspect that is investigated in thermal convection intensively [47].

### 3 Flow at low values of the Reynolds number $Re$

#### 3.1 Dimensionless Navier-Stokes equation and the Reynolds number

The various terms in the Navier–Stokes equation can be very different in magnitude, depending on the special flow under consideration. The Navier-Stokes equation is nonlinear and may exhibit turbulence in many situations [44, 45]. Analytical solutions of (65) exist only for simple geometries, especially in the limit of small values of the dimensionless *Reynolds number*  $Re$ , which we introduce now. Eq. (65) includes essentially three relevant parameters: the *kinematic viscosity*  $\nu = \eta/\rho$ , a typical length scale  $l$  (often the dimension of the container or of an swimming object) and a typical flow velocity  $u_0$ .

$$[\nu] = \frac{m^2}{s}, \quad [l] = m, \quad \text{and} \quad [u_0] = \frac{m}{s}. \quad (14)$$

These may be combined to the dimensionless Reynolds number

$$Re = \frac{u_0 l}{\nu} = \frac{\rho u_0 l}{\eta}, \quad (15)$$

which compares the inertia forces and the viscous ones. With  $u = u_0 \bar{u}$ ,  $x_i = l x'_i$ ,  $\bar{p} = p l / (\eta u_0)$  and a typical time  $t_0 = l / u_0$  with  $t = t_0 \bar{t}$  after multiplication of Eq. (65) by  $l^2 / (\eta u_0)$  one obtains

$$Re \left( \frac{\partial \bar{u}_i}{\partial \bar{t}} + \bar{u}_j \bar{\nabla}_j \bar{u}_i \right) = -\bar{\nabla}_i \bar{p} + \bar{\Delta} \bar{u}. \quad (16)$$

From this equation it is clear that the Reynolds number  $Re$  is the only parameter that indicates the importance of inertia relative to viscous forces. For two different fluids (for example with different viscosities) and two spheres with different radii in the same flow type the velocity

$\mathbf{u}/u_0$  depends in both cases on  $\mathbf{r}/l$  in the same manner, if the Reynolds numbers coincide. Flows which may be transformed into each other by such a similarity transformation are called similar fluids.

There are two flow regimes distinguishable:  $Re \ll 1$  and  $Re \gg 1$ . Usually, a flow becomes turbulent beyond a critical value of  $Re$  that depends on the flow type. In the range  $Re \ll 1$ , the term  $Re(\mathbf{u} \cdot \nabla)\mathbf{u}$  can be neglected and equation (65) reduces in the stationary Stokes or *creeping-flow equation*, which is in dimensional form

$$-\nabla p + \eta \nabla^2 \mathbf{u} + \mathbf{f} = 0. \quad (17)$$

The creeping-flow equation is particularly useful in describing the flow around colloidal particles because in this case the characteristic length  $l$  occurring in the Reynolds number can be identified with the particle size. Even for a colloidal particle as large as  $1 \mu\text{m}$  in water, assuming  $\rho = 10^3 \text{ kg m}^{-3}$ , the Reynolds number approaches unity at velocities of about  $1 \text{ ms}^{-1}$ . Hence for colloidal particles the condition  $Re \ll 1$  is almost always satisfied. It must be pointed out that even when the Reynolds number calculated using the size of a colloidal particle is usually less than one, the Reynolds number based on some macroscopic dimension of the flow (e.g. the diameter of a tube) can be much larger than one. Even in turbulent flow, if the particle is smaller than the microscopic scale of turbulence, the local flow in the neighborhood of a colloidal particle is laminar even though the “distant” velocity it experiences is a fluctuating function of time.

### 3.2 Example: Plane Poiseuille Flow

A flow induced by a pressure drop between two parallel plates is the so-called plane Poiseuille flow. If the two parallel plates are located at  $z = \pm d/2$  and parallel to the  $x - y$  plane we assume a pressure gradient along the  $x$ -direction and linear pressure drop  $\partial_x p = \text{const.}$ . Accordingly we expect a flow in  $x$ -direction  $\mathbf{u} = (u_x, 0, 0)$ . At the bounding plates we assume stick boundary conditions  $u_x(z = \pm d/2) = 0$  and therefore the only spatial dependence of the flow field is along the  $z$ -axis. In a stationary flow case  $\partial_t \mathbf{u} = 0$  and one has also  $(\mathbf{u} \cdot \nabla) = 0$ . Hence only the equation  $\eta \Delta u_x = \partial_x p = p_c$  is left. This is an ordinary differential equation of second order which may be solved by integration:  $u_x(z) = \frac{z^2}{2} (\partial_x p) / \eta + Cz$ . The problem is symmetric with respect to the reflection  $z \rightarrow -z$  and therefore  $C = 0$ . In order to fulfill the boundary conditions we have for the plane Poiseuille flow

$$u_x(z) = \frac{1}{2} \frac{p_c}{\eta} \left( z^2 - \left( \frac{d}{2} \right)^2 \right) \quad (18)$$

induced by the linear pressure drop  $p_c = \partial_x p$ . This laminar flow is only preferred for small values of the Reynolds number and at large values of  $Re$  one expects turbulent flows.

### 3.3 Particles in a Newtonian fluid

A particle suspended in a fluid starts to move by an applied force. For instance, if the particle has a higher density than the solvent, the particle sediments in a gravitational field.

The relation between the particle velocity and the applied force as well as the perturbation of the flow and the pressure field are calculated.



Every moving particle perturbs the flow field and this perturbation influences the motion of other particles. This effect of hydrodynamic interaction between moving and rather far distant particles (with a next neighbor distance much larger than the diameter of the particles) is described by the so-called Oseen tensor, as presented in the contribution of J. Dhont.

Particles in a local shear field rotate and this rotation perturbs the flow field too. This leads to a higher shear viscosity than for the fluid without particles.

**Hydrodynamic interaction between point particles.** – At a sufficiently large distance  $r$  from a moving sphere of radius  $R$ , i. e.  $R/r \ll 1$ , its action on the fluid is the same as that of a point force  $\delta(\mathbf{r})\mathbf{f}$  [1]. Assuming in the Stokes equation a point like body force  $\delta(\mathbf{r})\mathbf{f}$  at the origin

$$\nabla p = \eta \Delta u + \delta(\mathbf{r})\mathbf{f} \quad (19)$$

the flow field induced by this force is

$$\mathbf{u}(\mathbf{r}) = \boldsymbol{\Omega}(\mathbf{r}) \cdot \mathbf{f} = \frac{1}{8\pi\eta r} \left( \mathbf{I} + \frac{\mathbf{r} \otimes \mathbf{r}}{r^2} \right) \cdot \mathbf{f} \quad (20)$$

as shown in appendix B.  $\boldsymbol{\Omega}(\mathbf{r})$  is the so-called Oseen tensor.

**Equation for point particles** – Now we consider  $N$  moving point particles located at  $\mathbf{R}_i$  with a force  $\mathbf{F}_i$  acting on each of it and  $i = 1, \dots, N$ . Then the force density is

$$\mathbf{f}(\mathbf{r}') = \sum_{i=1}^N \delta(\mathbf{r}' - \mathbf{R}_i) \mathbf{F}_i \quad \text{usually } \mathbf{F}_i = \text{const.} \quad (21)$$

Together with the Oseen-tensor as defined by Eq. (20), the equation for the perturbed flow field in the presence of  $N$  particles is

$$\mathbf{u}'(\mathbf{r}) = \sum_{i=1}^N \boldsymbol{\Omega}(\mathbf{r} - \mathbf{R}_i) \cdot \mathbf{F}_i \quad (22)$$

The perturbation  $\mathbf{u}'(\mathbf{R}_i)$  at the place of the  $i$ -th particle is induced by all the other  $N - 1$  particles

$$\mathbf{u}'(\mathbf{R}_i) = \sum_{j \neq i} \boldsymbol{\Omega}(\mathbf{R}_i - \mathbf{R}_j) \cdot \mathbf{F}_j \quad (23)$$

For a creeping flow one assumes that a sphere adjusts due to stick boundary condition to the same velocity  $\dot{\mathbf{R}}_i = \mathbf{v}_i$  than the fluid in its immediate neighborhood  $\mathbf{u}(\mathbf{R}_i)$ . The flow field at the position of the  $i$ -th particle may have two contributions. The first contribution is the undisturbed flow field in the absence of particles  $\mathbf{u}_0(\mathbf{r})$ , such as for example the uniform flow field  $\mathbf{u}_0(\mathbf{r}) = \text{const.} \cdot \hat{\mathbf{n}}$  along some direction  $\hat{\mathbf{n}}$ , a linear shear field  $(\mathbf{u}_0)_x = sy$  or a parabolic shear profile, e.g. a plane Poiseuille flow with  $(\mathbf{u}_0)_x(y) = u_s(d^2 - y^2)$ . The second contribution,  $\mathbf{u}'(\mathbf{r})$ , is induced by all the other other moving particles. The force acting on the  $i$ -th particle

due to the Stokes law determines the velocity difference between this flow  $\mathbf{u}_0(\mathbf{r}) + \mathbf{u}'(\mathbf{r})$  and the actual velocity of the particle  $\mathbf{v}_i$

$$\mathbf{v}_i - [\mathbf{u}_0(\mathbf{R}_i) + \mathbf{u}'(\mathbf{R}_i)] = \frac{1}{6\pi\eta a} \mathbf{F}_i. \quad (24)$$

Here  $a$  is an effective radius of a point particle. For point particles the notion of an effective friction coefficient  $\zeta = 6\pi\eta a$  is also common. Hence, the equation of motion for the  $i$ th particle is

$$\begin{aligned} \dot{\mathbf{R}}_i \equiv \mathbf{v}_i &= \mathbf{u}_0(\mathbf{R}_i) + \mathbf{u}'(\mathbf{R}_i) + \frac{1}{6\pi\eta a} \mathbf{F}_i \\ &= \mathbf{u}_0(\mathbf{R}_i) + \sum_{j \neq i} \boldsymbol{\Omega}(\mathbf{R}_i - \mathbf{R}_j) \cdot \mathbf{F}_j + \frac{1}{6\pi\eta a} \mathbf{F}_i \\ &\equiv \mathbf{u}_0(\mathbf{R}_i) + \sum_{k=1}^N \mathbf{H}_{ik} \cdot \mathbf{F}_k, \end{aligned} \quad (25)$$

where

$$\mathbf{H}_{ik} = \begin{cases} \frac{1}{\zeta} \mathbf{1} & \text{for } k = i \\ \boldsymbol{\Omega}(\mathbf{R}_i - \mathbf{R}_k) & \text{for } k \neq i \end{cases} \quad (26)$$

is called the mobility matrix.

The forces acting on the particles may be induced for instance by gravitation or in the case of charged particles by an electric field. In bead spring models for polymers a part of the forces acting on the beads are due to the springs connecting next neighboring beads. Besides the hydrodynamic and spring forces in polymers thermal motion has to be taken into account as well. For more details about bead–spring models for polymers, where the hydrodynamic interaction is taken into account, see for instance Ref.[48] and the references cited therein.

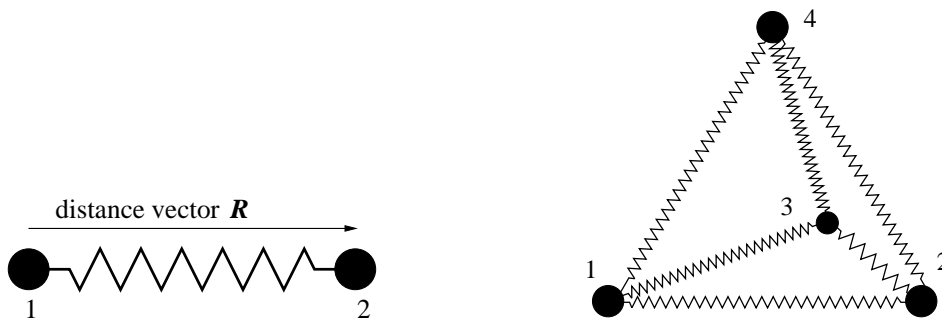


**Fig. 9:** Two simple bead–spring models: a) dumbbell and b) tetrahedron.

Two simple bead–spring models are the dumbbell and the tetrahedron as shown in Fig. 9. Both are used for modeling certain aspects of polymers. A simple potential for a linear spring with a finite equilibrium length  $b$  connecting two neighbor beads is

$$\Phi = \frac{1}{2}k(|\mathbf{R}| - b)^2 \quad (27)$$

with the force law

$$\mathbf{F}(\mathbf{R}) = -\nabla\Phi(R) = -k \left(1 - \frac{b}{|\mathbf{R}|}\right). \quad (28)$$

For such a spring potential the whole force acting on one bead of a tetrahedron or some complicated connected bead–spring model is

$$\mathbf{F}_j = k \sum_{i(\neq j)} \left(1 - \frac{b}{|\mathbf{r}_i - \mathbf{r}_j|}\right) (\mathbf{r}_i - \mathbf{r}_j). \quad (29)$$

This force together with Eq. (25) builds the equation of motion for the Stokesian dynamics of a bead spring system. More about Stokesian dynamics may be found in Ref. [27]. If the undisturbed flow  $\mathbf{u}_0(\mathbf{r})$  is a shear or a Poiseuille flow, a tetrahedron or another three–dimensional object is in permanent motion and rotation. Surprisingly, a tetrahedron migrates during its persistent rotating motion perpendicular to the streamlines [28] and moves to the center of the Poiseuille flow. Asymmetric dumbbells may migrate away from the center of the Poiseuille flow. So migration is the consequence of a delicate balance between different forces.

A simple consequence of the hydrodynamic interaction may be seen in Fig. 10. Here the force is calculated which is needed in order to keep the two beads fixed in a uniform flow of velocity  $\mathbf{u}$ . The force can be determined from equation (24) by setting the bead velocity  $\mathbf{v}_i = 0$ . Each bead perturbs the flow and reduces the flow velocity in its neighborhood. Therefore the dragforce on the second bead is reduced compared to that in absence of the first bead. This reduction depends on the distance between the two beads as can be seen from the dependence of the drag force as a function of the bead distance  $d$  in Fig. 10c). In both cases with the connection vector between the two beads either parallel or perpendicular to the flow, the forces needed to keep both beads fixed point into the direction opposite to the flow velocity. In the case of a finite value of  $\delta_x$  one has also to apply forces perpendicular to the flow.

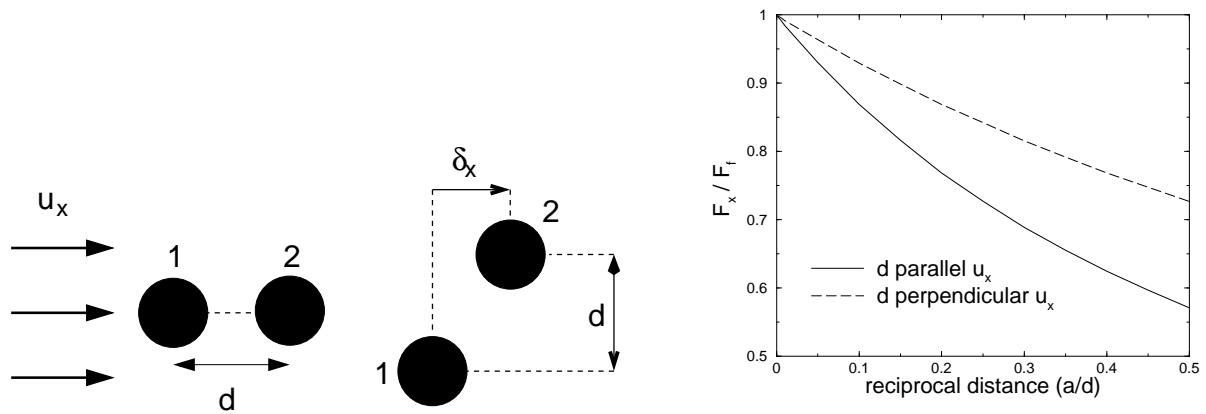


**Fig. 10:** Two beads kept fixed in a uniform flow, with the connecting vector either perpendicular or parallel to the flow direction  $\mathbf{u} = (u_x, 0, 0)$ . The drag force for each bead of the two bead system normalized to the drag force  $F_f = 6\pi\eta a$  needed for a single bead ( $F_f = 6\pi\eta a$ ). In the case of a perpendicular orientation we have chosen  $\delta_x = 0$ .  $a$  is the effective bead radius and  $d$  the distance between the beads.

### 3.4 Effect of a dilute suspension of particles on the shear viscosity

Small particles (either solid, liquid, or gaseous) that are randomly dispersed throughout another fluid material are quite common in nature and industry. The term *suspension* or colloidal suspension usually refers to a system of small solid particles in a liquid, but the nature of the two media is not of particular significance from the dynamical point of view and our use of the word here will include also systems of drops of one liquid dispersed either in another liquid (an emulsion) or in a gas. How do such suspensions behave in response to applied forces and moving boundaries like in shear cells? How does a suspension influence the shear viscosity? A. Einstein has shown in 1906 for the first time that suspended particles increase the shear viscosity compared to the pure solvent [19, 1] as described by the following formula

$$\eta = \eta_0 \left( 1 + \frac{5}{2} \varphi \right) \quad \text{with} \quad \varphi = \frac{4\pi R^3}{3} c, \quad (30)$$

$\varphi$  being the part of the volume occupied by the suspended particles and  $\eta_0$  is the shear viscosity of the pure solvent. This contribution is obtained in the very diluted limit, where particles do not interact via hydrodynamic interactions. For the calculations the fluid was assumed to be incompressible and particles were assumed to be spherical.

If the suspended particles are deformable, such as vesicles, then the situation is slightly different as shown recently [20]. Vesicles in shear flow are of elliptical shape and the larger principal axis is obliquely oriented with respect to the parallel flow lines. The inclination angle depends on the shear rate. The shear viscosity of a fluid with suspended vesicles is

$$\eta_{eff} = \eta \left[ 1 + \frac{5}{2} \varphi \frac{23\lambda - 16}{23\lambda + 32} + \varphi \left( \frac{15}{8\pi} \right)^{1/2} \frac{(4h^2 - \Delta)}{h} \right]. \quad (31)$$

Here  $\lambda = \bar{\eta}/\eta$  is the viscosity contrast, with  $\eta$  the viscosity of the solvent and  $\bar{\eta}$  the viscosity of fluid in the vesicle.  $\Delta$  is the excess area.  $\Delta = 0$  for a spherical vesicle and  $h = 60\sqrt{2\pi/15}(32 + 23\lambda)$ . Since in many cases  $4h^2 - \Delta < 0$  the shear viscosity of suspended vesicles is less than for hard spherical particles.

So far sufficiently diluted particle suspensions have been considered in shear flow where the hydrodynamic interaction between particles is sufficiently small and where the particles behave like independent ones. As we have seen above, if two spheres come close enough, say if the ratio between the particle diameter  $2R$  and the distance  $d$ ,  $R/d$ , becomes larger, then the drag on one of them is influenced by a second sphere nearby: The spheres experience in this case a *hydrodynamic interaction*. Such interactions between two spheres lead to a contribution to the viscosity  $\bar{\eta}$  that is proportional to  $\varphi^2$ . This effect of two body interactions on  $\bar{\eta}$  was computed by Batchelor [49]. Here, in contrast to the hydrodynamic interaction according to the Oseen tensor, which describes the interaction of point particles, also the particle rotations have to be taken into account for the determination of the particle interactions. When combined with Einstein's result the calculation in Ref.[49] gives

$$\bar{\eta} = \eta_0 \left( 1 + \frac{5}{2} \varphi + 6.2 \varphi^2 \right). \quad (32)$$

For polystyrene spheres this formula holds good up to a concentration  $\varphi \leq 0.10$ .



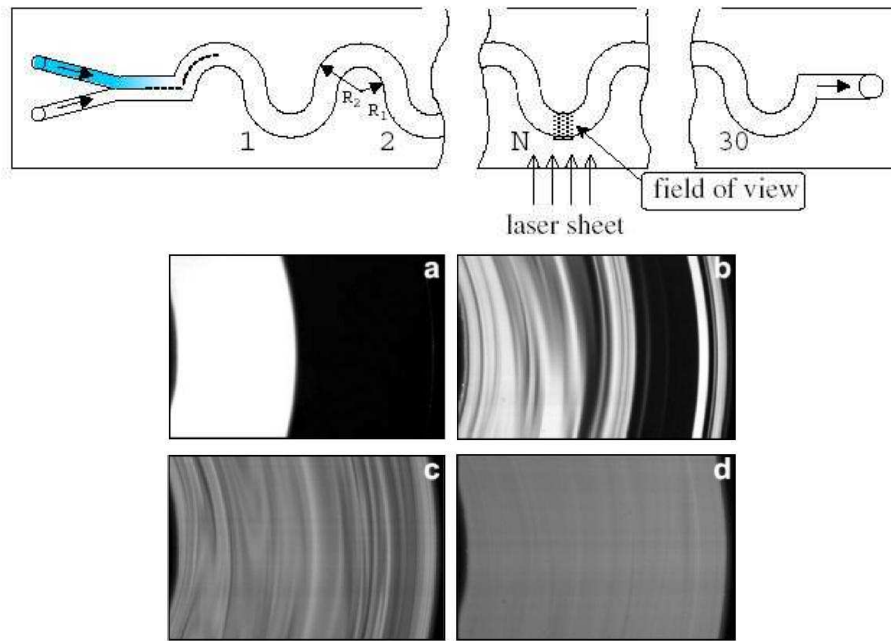


**Fig. 11:** The top part is a sketch of the experiment. Parts a-d show different mixing states of the two fluids at different positions along the pipe (see text) [50].

### 3.5 Elastic turbulence in polymeric solutions at small $Re$

Polymers with a relaxation time  $\tau$  in a local velocity gradient with a shear rate  $s$  cannot relax to their equilibrium shape if the Weissenberg number  $s\tau > 1$  becomes much larger than one. Polymers in a shear gradient tumble with a rather stochastic behavior of the mean extension of the polymer [51]. Adequate shear rates can be achieved with laminar flow in micro channels. However, not only the shape of polymers is deformed in a shear flow. A dynamical shape change and the tumbling influence also the local flow field around the polymer. This influence will increase with the density of the polymers. With the density of the polymers also the hydrodynamic interaction (via the Oseen tensor) between the polymers increases, which affects also their dynamics. The action of a shear rate on polymers and the back action of many polymers on the flow field can cause turbulent flows and this already at rather small values of Reynolds number  $Re = 0.01..1$  [52, 50]. This phenomenon has been called elastic turbulence.

This elastic turbulence is also employed for mixing in micro channels [53, 50]. This is shown in Fig. 11 where fluid mixing in a pipe is studied without and with polymers in the fluids. In this experiment the Weissenberg number  $Wi = 6.7$  was chosen. In the bottom part of Fig. 11(a) it is demonstrated that two Newtonian fluids do not mix even after the curve  $N = 29$ . With a finite amount of polymers both fluids, which are injected separately, mix with increasing distance from the left end as can be seen in parts (b)-(d). The shape shots (b)-(d) are obtained at  $N = 8, 29, 54$ . The efficiency of mixing with polymers is evident. A good theoretical description of the mechanism is missing up to now.

## 4 Nematic liquid crystals

Complex fluids are deformable materials which have, compared with simple fluids, further inner degrees of freedom. In order to describe these additional degrees of freedom the equations of motion for simple fluids must be generalized and coupled with further equations. For a two component fluid mixture, such as e.g. water–alcohol, one needs for each component a conservation law for mass. However, instead of two conservation laws for mass one may use a conservation law for the whole mass and an equation for the concentration of one fraction. In charged systems one has in addition a conservation law for the charge

$$\dot{\rho}_e + \nabla \cdot \mathbf{j}^{(e)} = 0 \quad (33)$$

with the electrical current density  $\mathbf{j}^{(e)}$ .

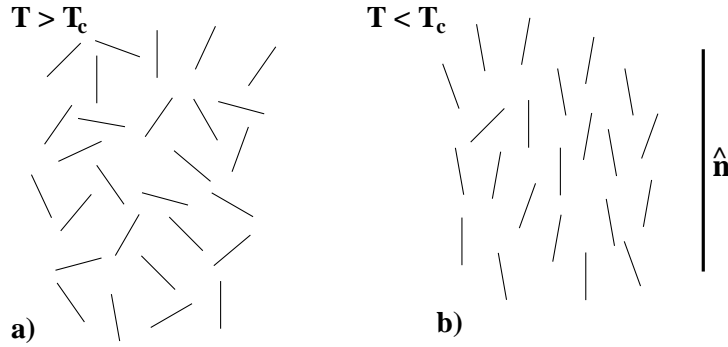


**Fig. 12:** a) Disordered (isotropic) phase beyond the isotropic–nematic transition ( $T > T_c$ ) and the phase with orientational order (nematic phase) below the nematic–isotropic phase transition ( $T < T_c$ ).  $\hat{\mathbf{n}}$  is the director.

In systems that have many components conservation laws completely determine the set of hydrodynamical variables. For liquid crystals or superfluids there are one or more variable associated with broken symmetries. In a nematic liquid crystalline phase one has an additional spontaneously broken rotational symmetry. Organic liquids may become anisotropic due to an orientational ordering of non spherical molecules. The angle distribution of the anisotropic molecules is uniform in the isotropic phase, cf. Fig. 12 a), but in the anisotropic nematic phase the angle distribution exhibits a local maximum and this preferred direction is described by the director field  $\mathbf{n}(\mathbf{r}, t)$ . The director field has a  $\pm$ -symmetry ( $\mathbf{n} = -\mathbf{n}$ ) and hence in the nematic phase the rotational symmetry is broken. Since this symmetry is spontaneously broken (broken during a phase transition) without application of external fields, it is called a *spontaneously broken symmetry*. Similar as in simple fluids there is no positional order of the molecules in nematic liquid crystals. In the absence of boundaries every spontaneously formed direction has the same energy, as long as the orientation of the director  $\mathbf{n}$  is everywhere the same. Therefore, rigid rotations of the whole fluid volume don't cost energy in the absence of boundaries.

Related to the orientational ordering of the molecules is the anisotropy of material properties. The dielectric constant is different for a light wave with the wave vector  $\mathbf{k}$  parallel to  $\mathbf{n}$  ( $\varepsilon = \varepsilon_{\parallel}$ ) and perpendicular to  $\mathbf{n}$  ( $\varepsilon = \varepsilon_{\perp}$ ). The same holds for the index of refraction, which is also

different parallel to  $\mathbf{n}$  ( $n = n_{\parallel}$ ) and perpendicular to  $\mathbf{n}$  ( $n = n_{\perp}$ ). Due to the anisotropy,  $\Delta n = n_{\parallel} - n_{\perp}$ , nematic materials are birefringent.

Only spatially varying deformations of the director field  $\mathbf{n}(\mathbf{r})$  lead to a change (increase) of the free energy. Therefore spatial deformations tend to relax to the homogeneous director orientation and if the wavelength of the deformations becomes larger and larger, the relaxation time increases too. Therefore, the deformation of the director field is an additional hydrodynamic mode in nematic liquid crystals and the equations must be generalized accordingly: To any spontaneously broken continuous symmetry, there is a symmetry variable behaving hydrodynamically,  $\omega(k \rightarrow 0) \rightarrow 0$ .

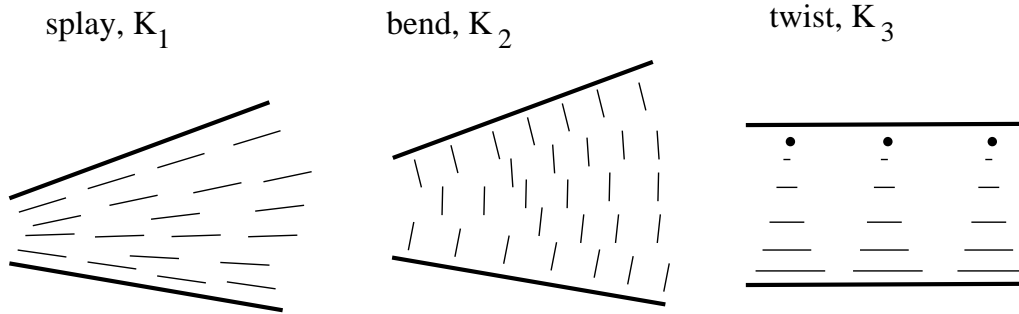


**Fig. 13:** The three fundamental distortions of the nematic director field  $\mathbf{n}(\mathbf{r}, t)$ : a) splay, b) bend and c) twist deformation.

Changes of the director field  $\delta n_i$  are not conserved. The deformations of the director field are elastic and any deformation can be decomposed in three fundamental deformations, the splay, the bend and the twist deformation, cf. Fig. 13. The energy stored in each deformation is proportional to an elastic constant:  $K_1$  the splay elastic constant,  $K_2$  the twist elastic constant and the bend elastic constant  $K_3$ . The Frank free energy of the director deformations is

$$\mathcal{F} = \frac{1}{2} \int d^3r \left( K_1 (\nabla \cdot \mathbf{n})^2 + K_2 [\mathbf{n} \cdot (\nabla \times \mathbf{n})]^2 + K_3 [\mathbf{n} \times (\nabla \times \mathbf{n})]^2 - \varepsilon_0 \varepsilon_a (\mathbf{n} \cdot \mathbf{E})^2 \right) \quad (34)$$

with  $\varepsilon_a = \varepsilon_{\parallel} - \varepsilon_{\perp} > 0$ . The last contribution describes the coupling to an applied electric field. For  $\varepsilon_a > 0$  a parallel alignment between the director field and the electric field reduces the free energy. If a magnetic field is applied, the free energy contribution  $-\varepsilon_0 \varepsilon_a (\mathbf{n} \cdot \mathbf{E})^2$  has to be replaced by  $-\chi_a (\mathbf{n} \cdot \mathbf{H})^2$ . A detailed derivation of this free energy for the distortions of the director field and the respective equation of motion for  $\mathbf{n}(\mathbf{r}, t)$  may be found in the books [54, 31, 55].

The orientation of the director close to a container boundary depends on the surface preparation. There are several surface preparation techniques which induce close to the boundary an orientation of  $\mathbf{n}$  either parallel or perpendicular or with some oblique angle with respect to the container boundary. Due to the elastic energy of orientational deformations of the director field the orientation of  $\mathbf{n}$  at the boundaries is transmitted to the bulk. An example is shown for a sandwich geometry in Fig. 14a) with the orientation of the director parallel to the wall and with the same orientation at both walls. The result is a homogeneous orientation of  $\mathbf{n}$  in the bulk. If an electric field is applied, as indicated in Fig. 14b), and if the material has a positive dielectric

anisotropy,  $\varepsilon_a > 0$ , the energy is decreased when  $\mathbf{n}$  and  $\mathbf{E}$  become parallel. This orientation effect of the applied electric field competes with the boundary induced director orientation. As long as the effect is weaker as the boundary orientation effect,  $\mathbf{n}$  stays parallel to the wall. However, the electric field can distort the director in the bulk. Since in this configuration the electric field is perpendicular to the initial orientation, a critical electrical field is required. This field driven orientation transition in the bulk is the so-called Fredericks transition. If the electric field is switched off, the director relaxes back to the initial configuration. Since the nematic liquid crystal is birefringent its optical properties can be changed by switching on and off by an electric field or a voltage between the two bounding plates. The initial configuration in an LCD is a twisted state, but the LCD is switched by the same mechanism.

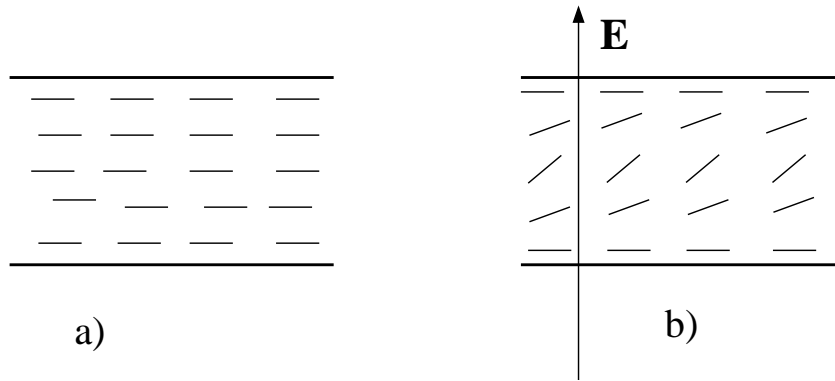


**Fig. 14:** a) Homogeneous director orientation induced by the boundary orientation. b) The director is distorted in the bulk by application of an electric field (Fredericks transition).

**Viscosity in a uniaxial liquid - anisotropic viscosity –** Due to the orientational order the viscosity depends on the orientation of the director  $\mathbf{n}$  with respect to the shear plane. As we have seen the orientation of the director can be enforced by application of a magnetic or electric field. Hence we will assume that the director is strongly aligned along the  $x_3 = z$ -direction, cf. Fig. 15. In this case the expressions for the linear shear stresses are

$$\begin{aligned} \sigma'_{12} = \sigma'_{21} &= \eta_3 \left( \frac{\partial u_1}{\partial x_2} + \frac{\partial u_2}{\partial x_1} \right), \\ \sigma'_{23} &= \eta_4 \frac{\partial u_2}{\partial x_3} + \eta_1 \frac{\partial u_3}{\partial x_2}, \quad \sigma'_{32} = \eta_2 \frac{\partial u_2}{\partial x_3} + \eta_4 \frac{\partial u_3}{\partial x_2}, \end{aligned} \quad (35)$$

$$\sigma'_{31} = \eta_4 \frac{\partial u_3}{\partial x_1} + \eta_2 \frac{\partial u_1}{\partial x_3}, \quad \sigma'_{13} = \eta_1 \frac{\partial u_3}{\partial x_1} + \eta_4 \frac{\partial u_1}{\partial x_3}, \quad (36)$$

The four viscosities  $\eta_1$ ,  $\eta_2$ ,  $\eta_3$  and  $\eta_4$  constitute four of five independent viscosities in an uniaxial system. Note that the coefficient of  $\partial u_2 / \partial x_3$  in the equation of  $\sigma'_{23}$  and the coefficient of  $\partial u_3 / \partial x_2$  in the equation of  $\sigma'_{32}$  are (like the corresponding coefficients in the last equation) identical. Their identity, which constitutes the only surprise of the three equations above, is an example of an *Onsager relation*, and readers who are unfamiliar with Onsager relations and with the subject of irreversible thermodynamics in which they arise, should take it on trust or should read in the books of deGennes/Prost [55], of Landau [54], of Chaikin/Lubensky [31] or

the original literature about nematic liquid crystals. These five viscosities have been measured at least for two substances.

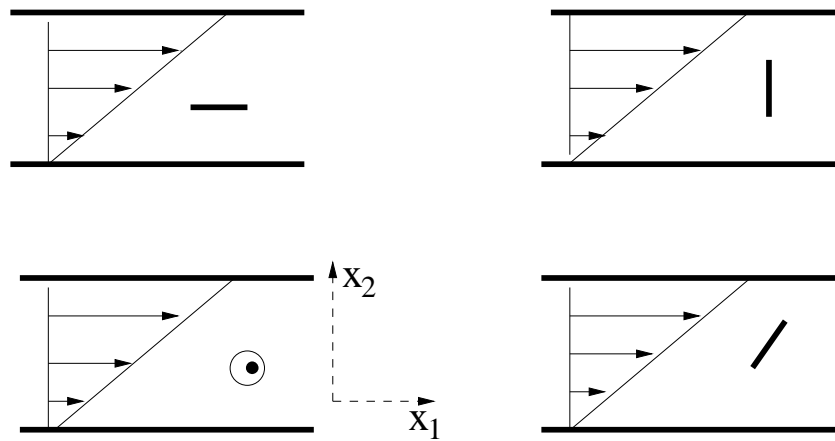


**Fig. 15:** *Measuring different shear viscosities for different orientations of the nematic director with respect to the shear plane.*

If there are deformations of the director field, their relaxations excite a flow and any flow influences the orientation of the director field. Therefore in the equation for the momentum conservation there are contributions due to the director deformation and in the dynamic equation for the director  $\mathbf{n}$  the shear fields  $\partial_i u_j$  occur. Due to the many material parameters in nematics the equations look much more complicated than the Navier–Stokes equation, but they are solvable and all the material parameters may be measured. The systematic derivation of the equations for nematodynamics is described in [55, 7, 54]. Since the director field is a local unit vector ( $\mathbf{n}^2 = 1$ ), the dynamics of the director field is restricted to rotations, therefore  $\dot{n}_i n_i = 0$ .

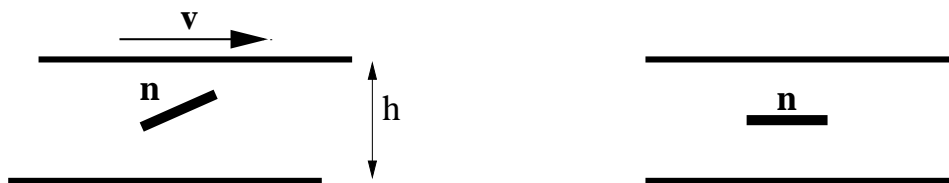


**Fig. 16:** *Flow alignment of the director field in the center of the plane shear cell.*

The mean orientation of the molecules close to container boundaries depends on the preparation of the surface. Assume that the surfaces of the shear cell are coated in that way that the molecules align parallel to the container boundaries. If the upper plate is moved with some velocity  $\mathbf{v}$  the director is still undistorted close to the upper and the lower plate, but in the center of the shear cell the director field becomes distorted and non-parallel to the bounding walls as indicated in Fig. 16. Vesicles show a similar inclined flow alignment in shear flow [25]. Suspended non spherical objects may be oriented in shear fields by similar mechanisms. About flow effects in further liquid crystal phases see [55, 7].

## 5 Polymer liquids

The viscosities of polymer liquids show both elastic and viscous behavior. Nematic liquid crystals are elastic with respect to their orientational order. The elasticity of polymer solutions is due to the entropic elasticity of the polymers which resembles the elasticity of a solid with respect to positional deformations. On a short time scale (high frequencies) the elastic behavior is pronounced and on a long time scale (small frequencies) the viscous behavior. The notion high and low frequency depends on the material and its internal relaxations. With increasing excitation frequencies any material exhibits elastic behavior beyond some critical frequency or below a certain time scale. In polymer liquids the relaxation of polymers may be that slow that the slow dynamics of individual polymers may interfere with the slow macroscopic hydrodynamic modes. In the regime where both time scales overlap viscoelasticity arises.

A hydrodynamic theory of simple or multicomponent fluids relies on conservations laws. Systems with spontaneously broken symmetries take into account the dynamical equations for broken-symmetry hydrodynamic variables. In both cases the fast dynamics at molecular level adjusts immediately to the far slower hydrodynamic motion. For viscoelastic fluids one has to couple the slow hydrodynamic modes (slow in terms of the dynamics at the molecular level) to appropriate slow modes of the microscopic dynamics. This field of viscoelastic fluids is less mature than hydrodynamic theories for simple fluids and for liquids with spontaneously broken symmetries.

Various models for viscoelastic fluids exist, but a general theory is not available at present. Only for small deformations of the viscoelastic fluids there is with the linear Maxwell model a reasonable model available.

### 5.1 Linear Viscoelasticity - Maxwell Model

Let us consider a symmetric deformation field

$$E_{ij} = \frac{1}{2} (\nabla_i w_j + \nabla_j w_i) \quad (37)$$

with  $w_i = r_i - r'_i$  being the difference between  $r_i$  the final and  $r'_i$  the initial position of a fluid element. This symmetric deformation tensor does not include simple rotations. For small deformations, which we will only consider in this section, the field  $E_{ij}$  is related to the stress tensor via Hooke's law. However, after a certain time polymers or some particle arrangements relax to a new equilibrium configuration and the elastic stress contribution relaxes too. This is different to a solid where the stress only relaxes when all the atoms or molecules relax to their fixed equilibrium positions.

Therefore in a viscoelastic liquid one has the shear stress and a relaxing elastic stress. This suggests the following equation of motion for the stress tensor in the case of small fluid deformations

$$\sigma_{ij} + \lambda_1 \frac{\partial}{\partial t} \sigma_{ij} = \eta \dot{\gamma}_{ij}. \quad (38)$$

It is the so-called Maxwell model for linear viscoelastic fluids. For simplicity we have only one relaxation constant  $\lambda_1$ . This is a first order inhomogeneous and linear differential equation for

the stress tensor, which may be easily integrated

$$\sigma_{ij} = e^{-t/\lambda_1} \left[ \int \left( -\frac{\eta}{\lambda_1} \dot{\gamma}(t') e^{t'/\lambda_1} dt' \right) + C_{ij} \right]. \quad (39)$$

This solution of the Maxwell model shows a memory behavior that is typical for a viscoelastic fluid. Especially the memory effects due to elastic behavior make a continuum formulation of the viscoelastic fluids intricate.

With a periodic shear field  $\dot{\gamma} = \omega \gamma_0 \cos(\omega t)$  and the relation  $\sigma(t) = \gamma_0 G(t)$  used together with Eq. (38), the expressions for the loss  $G'(t)$  and the storage modulus  $G''(t)$  read

$$G'(\omega) = \frac{\eta \lambda_1 \omega^2}{1 + \lambda_1^2 \omega^2} \quad \text{and} \quad G''(\omega) = \frac{\eta \omega}{1 + \lambda_1^2 \omega^2}. \quad (40)$$

From measurements with oscillatory shear one can determine the two unknown parameters, the shear viscosity  $\eta$  and the relaxation  $\lambda_1$  in the Maxwell model.

## 5.2 Nonlinear deformations of viscoelastic fluids

Most of the flow problems of viscoelastic fluids cannot be described by the linear Maxwell model, c.f. Eq. (38). In a flow of a Newtonian fluid the temporal change of a field has two contributions described by the substantial derivative:  $d/dt = \partial/\partial t + (\mathbf{u} \cdot \nabla)$ . We assume here at some initial time the distance  $|\delta \mathbf{r}| = |\mathbf{r}_1 - \mathbf{r}_2|$  between two fluid elements. At some time later the positions of the fluid elements might have changed to  $\delta \mathbf{r}' = \mathbf{r}'_1 - \mathbf{r}'_2$  and the distance is very likely not the same anymore  $|\delta \mathbf{r}'| \neq |\delta \mathbf{r}|$ . This does not have any consequence for a Newtonian fluid, only energy has been dissipated during the motion relative to each other. In a viscoelastic fluid such a change of the distance between neighboring fluid elements means an elastic deformation that contributes to the stress tensor. The time derivative of the stress tensor in viscoelastic fluids must be changed accordingly.

It is known from classical mechanics that time derivatives of vector or tensor components in a moving frame of reference obey special transformation rules. In continuum mechanics there are two common formulations of the time derivative for the stress tensor (see e.g. [26])

$$\dot{\sigma}' \rightarrow \frac{D}{Dt} \sigma' = \partial_t \sigma' + (\mathbf{u} \cdot \nabla) \sigma'_{ij} - \sigma'_{ij} \cdot \nabla \mathbf{u} - (\nabla \mathbf{u})^\dagger \cdot \sigma' \quad (41)$$

with  $(\nabla \mathbf{u})_{ij} = \partial_i u_j$ . Here  $\dot{\sigma}'$  denotes the time derivative in the local frame of reference of a fluid element, where the partial derivatives on the right hand side refer to space and time coordinates in a fixed frame of reference. This is known as the (*upper*) *convected derivative*. Alternatively one has with

$$\dot{\sigma}' \rightarrow \frac{\hat{D}}{\hat{D}t} \sigma' = \partial_t \sigma' + (\mathbf{u} \cdot \nabla) \sigma'_{ij} - \sigma'_{ij} \cdot (\nabla \mathbf{u})^\dagger - (\nabla \mathbf{u}) \cdot \sigma' \quad (42)$$

also the (*lower*) *convected derivative*. In the traditional literature the upper convected derivative is preferred and this is justified by the so-called *material frame independence*. Recently, however, it was argued that the lower convected is the appropriate one, because it provides the

appropriate limit of an elastic solid [56].

With this definition one obtains with (38) either the upper or lower convected Maxwell model

$$\sigma' + \lambda \frac{D}{Dt} \sigma' = \eta \dot{\gamma}. \quad (43)$$

This model has been applied to various situations, but with the continuum formulation of the equations of motion of viscoelastic fluids there is besides the appropriate choice of the time derivative the question about the appropriate macroscopic description of the polymer deformations. In other words, what are appropriate additional contributions on the right hand side of Eq. (43) in order to describe for instance the viscoelasticity of flow in polymer solutions? There are a number of models used in the literature, but a heuristic approach with a similar fundamental importance as the Navier–Stokes equation for Newtonian fluids, is not available yet.

### 5.3 Example: Pipeflow for a shear thinning fluid

In a number of complex fluids one observes shear thinning behavior, i.e. the viscosity decreases with increasing shear rate. There is no general theory for viscoelastic fluids, but there are a number models for special flow situations.

For instance, for many viscoelastic fluids a shear–rate–dependence of the viscosity occurs when the shear rate is high enough to disturb the equilibrium distribution of the inter particle spacing and the particles cannot relax fast enough. The rate at which the particle equilibrium is regained is controlled by the particle diffusivity, given in dilute solution by

$$D_0 = \frac{k_B T}{6\pi\eta R}. \quad (44)$$

The time  $t_D$  for a particle to diffuse a distance equal to its Radius  $R$  is therefore

$$t_D \sim \frac{R^2}{D_0} = \frac{6\pi\eta R^3}{k_B}. \quad (45)$$

The shear rate has the dimension 1/time, therefore one can define a dimensionless shear rate, or *Peclet number*, as

$$\text{Pe} = \frac{\eta \dot{\gamma} R^3}{k_B T} \propto \dot{\gamma} t_D. \quad (46)$$

With  $\tau_R$  the relaxation time of polymers in solution, a polymer in a large enough shear field with

$$\dot{\gamma} \tau_R > 1 \quad (47)$$

cannot adjust to its equilibrium coiled shape as well. Hence shear thinning may also occur in polymer solutions.

In the range of large shear rates, this shear rate dependent viscosity may be described by an approximate ”power-law” expression

$$\eta(\dot{\gamma}) = m \dot{\gamma}^{n-1} \quad (48)$$



with  $n$  from the interval  $n = 0.15 \dots 0.8$ . Obviously, this shear rate dependent viscosity may change the flow, e.g. through a pipe.

Stationary flows of shear rate dependent complex fluids, such as a stationary pipe flow, may be described by the Navier-Stokes equation with a shear rate dependent viscosity. The stationary form of equation (65) for a shear rate dependent viscosity and incompressibility is

$$0 = -\partial_{x_i} p + (\partial_{x_k} \eta) (\partial_{x_k} u_i + \partial_{x_i} u_k) + \eta \partial_{x_k}^2 u_i. \quad (49)$$

With the axis of the pipe along the  $z$ -axis the velocity in the pipe is  $\mathbf{u}(r) = (0, 0, u_z(r))$ . With the Laplacian and the gradient in cylindrical coordinates (only the  $r$  dependent part is shown)  $\Delta u_z = \frac{1}{r} \partial_r (r \partial_r u_z)$  and  $\nabla f(r) = \hat{e}_r \partial_r f(r)$  one obtains

$$\frac{p_0 - p_L}{L} = \frac{1}{r} \frac{d}{dr} \left( r \eta \frac{du_z}{dr} \right) \quad (50)$$

with the pressure drop  $(p_0 - p_L)$  along the pipe of length  $L$ . With  $\dot{\gamma} = \partial_r u_z$  and  $\eta$  from (48) an integration with respect to  $r$  yields

$$m \left( \frac{du_z}{dr} \right)^n = \frac{(p_0 - p_L)r}{2L} + \frac{C_1}{r}. \quad (51)$$

Since the shear rate on the axis of the pipe at  $r = 0$  is finite or zero (symmetry) the constant  $C_1$  must vanish. With  $\tau_R = \frac{(p_0 - p_L)R}{2L}$  one has

$$m \left( \frac{du_z}{dr} \right)^n = \tau_R \frac{r}{R}. \quad (52)$$

Integration of this equation gives the velocity-profile

$$u_z = - \left( \frac{\tau_R}{mR} \right)^{1/n} \frac{r^{1+\frac{1}{n}}}{1+\frac{1}{n}} + C_2. \quad (53)$$

Since the flow velocity vanishes at the pipe wall  $u_z(r = R) = 0$  (stick boundary condition) it follows with the constant  $C_2$  from this condition

$$u_z = \left( \frac{\tau_R}{mR} \right)^{1/n} \frac{R}{1+\frac{1}{n}} \left[ 1 - \left( \frac{r}{R} \right)^{\frac{1}{n}+1} \right]. \quad (54)$$

One should remember that the power-law behavior of the viscosity is an approximation that holds only for large enough shear rates (therefore close to the pipe boundary).

In the limit  $n \rightarrow 0$  the flow velocity  $U(r) = u_z(r)/\langle u_z(r) \rangle$  becomes a constant besides a small range close to the wall, where the shear rate diverges  $\frac{d}{dr} u_z(r \sim R) = -(\tau_R/m)^{1/n}$ .

In addition the volume rate  $Q$  going through the pipe is of high practical relevance

$$\begin{aligned} Q &= \int_0^{2\pi} d\varphi \int_0^R u_z(r) r dr d\varphi \\ &= 2\pi R^2 \int_0^1 u_z \frac{r}{R} d\left(\frac{r}{R}\right) = \frac{\pi R^3}{\frac{1}{n} + 3} \left( \frac{\tau_R}{m} \right)^{1/n} \\ &= \frac{\pi R^3}{\frac{1}{n} + 3} \left( \frac{(p_0 - p_L)R}{2mL} \right)^{1/n}. \end{aligned} \quad (55)$$

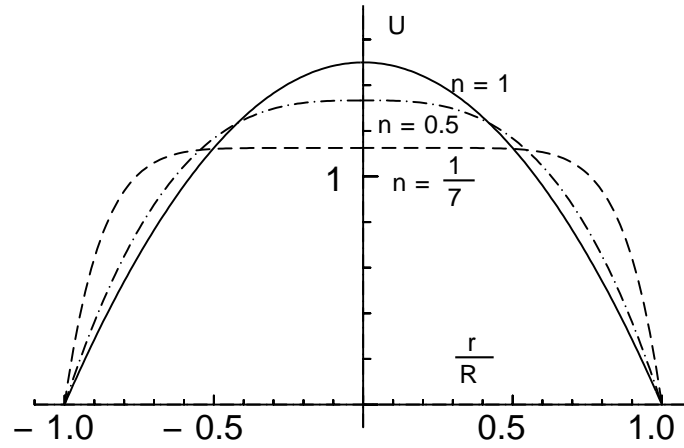


**Fig. 17:** The velocity  $U = u_z(r)/\langle u_z(r) \rangle$  normalized to the average velocity  $\langle u_z(r) \rangle$  is shown for the Newtonian fluid  $n = 1$ , for  $n = 1/2$  and  $n = 1/7$ .

For  $n = 1$  and  $m = \eta$  this reduces to the Hagen-Poiseuille equation for laminar flow of Newtonian fluids through a pipe. Rather interesting is also  $Qm/\tau_R$ , which is independent of the pressure drop for Newtonian fluids whereas for non-Newtonian fluids one has

$$\frac{Qm}{\tau_R} \sim (p_0 - p_L)^{(1-n)/n}. \quad (56)$$

For large pressure drops the volume rate for non-Newtonian fluids may be much higher than for Newtonian fluids. However, this conclusion holds only as long as the fluid is laminar and not turbulent. In the turbulent regime the so called turbulent drag reduction occurs, i.e. the mean flow velocity through pipes of liquid with polymer additives is higher than with without polymer additives. This effect still not understood in a satisfying manner.

## Appendix

### A Equations of motion for Newtonian fluids

The dynamics of a Newtonian fluid is described by a velocity field  $\mathbf{u}(\mathbf{r}, t)$ , by the mass density  $\rho(\mathbf{r}, t)$  the temperature field  $T(\mathbf{r}, t)$  and the pressure field  $p(\mathbf{r}, t)$ .

According to Newton's law there are three equations for the momentum density  $\mathbf{g}(\mathbf{r}, t) = \rho(\mathbf{r}, t) \mathbf{u}(\mathbf{r}, t)$

$$\frac{\partial g_i}{\partial t} + (\mathbf{u} \cdot \nabla) g_i = -\nabla_i p + \nabla_j \sigma'_{ij} + \rho f'_i. \quad (57)$$

Here the right hand side includes volume forces which are the hydrostatic pressure gradient  $\nabla_i p$ , the divergence of the viscous stress tensor  $\sigma'_{ij}$  and an external force per unit volume  $f'_i$ .  $f'_i$  may be due to an electric field in charged fluids or due to gravitation.

The interactions of a fluid element with its neighborhood are expressed in terms of a stress tensor  $\sigma_{ij}$  that includes both the pressure and the viscous stress. Consider a small volume element as

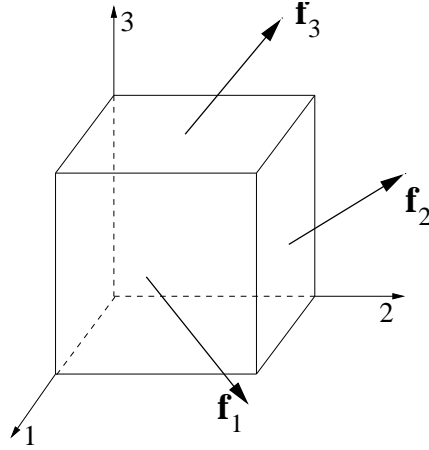


**Fig. 18:** The force per area acting onto the plane perpendicular to the  $i$ -axis is  $\mathbf{f}_i = (\sigma_{i1}, \sigma_{i2}, \sigma_{i3})$ .  $\sigma_{ii}$  is the normal component and  $\sigma_{ij}$  ( $i \neq j$ ) are the force densities in the planes.

shown in Fig. 18, with forces per area  $f_i$  acting on its surfaces. These forces form a stress tensor  $\sigma_{ij}$  with  $\mathbf{f}_i = (\sigma_{i1}, \sigma_{i2}, \sigma_{i3})$  and integrating the forces over the whole surface gives via Gauss's integral theorem

$$\oint_{\partial V} d\mathbf{S}_j \sigma_{ij} = \int_{\Delta V} dV \partial_j \sigma_{ij} = \Delta V \partial_j \sigma_{ij}. \quad (58)$$

The stress  $\sigma'_{ij}$  due to the velocity differences between neighboring fluid elements can be obtained by separating the isotropic stress contribution,  $-p\delta_{ij}$ , from the total stress  $\sigma_{ij}$ . An expansion of the viscous part of the stress tensor,  $\sigma'_{ij}$ , depends only on two viscosities and is of the following form <sup>1</sup>

<sup>1</sup>The stress tensor of a fluid,  $\sigma'_{ij}$  is only different from zero, if viscous friction occurs in a fluid. This is the case for real fluids and non-vanishing velocity gradients, when different parts of the fluid move with different velocities. An expansion of the stress tensor up to the leading order of the gradients is

$$\sigma'_{ij} = \eta_{ijkl} \nabla_k u_l, \quad (59)$$

whereby  $\eta_{ijkl}$  is the fourth rank viscosity tensor. This fourth rank tensor is the most general transformation between the two second rank tensors  $\sigma'_{ij}$  and  $\nabla_k u_l$ . One may check that the entropy production due to the viscous dissipation is proportional to  $\eta_{ijkl} \nabla_i u_j \nabla_k u_l$  and therefore the viscosity tensor must be invariant against the replacement  $kl \rightarrow ij$ .  $\sigma_{ij}$  must also vanish in the case of rigid rotation of the fluid (there is no viscous friction related). Therefore  $\sigma'_{ij}$  includes only symmetric combinations of the derivatives  $\nabla_k u_i + \nabla_i u_k$ , (the antisymmetric combinations describe rotations). Since  $\sigma'_{ij}$  must be symmetric the following identities must hold

$$\eta_{ijkl} = \eta_{klij} = \eta_{jikl} = \eta_{jilk}. \quad (60)$$

There are only two combinations of the Kronecker  $\delta_{ij}$

$$\delta_{ij}\delta_{kl} \quad \text{and} \quad \delta_{ik}\delta_{jl} + \delta_{il}\delta_{jk} \quad (61)$$

which fulfill this symmetry. Therefore the viscosity tensor includes two independent coefficients

$$\eta_{ijkl} = \eta \delta_{ij}\delta_{kl} + \zeta (\delta_{ik}\delta_{jl} + \delta_{il}\delta_{jk}). \quad (62)$$

$$\sigma'_{ij} = \eta \left( \nabla_i u_j + \nabla_j u_i - \frac{2}{3} \delta_{ij} (\nabla \mathbf{u}) \right) + \zeta \delta_{ij} \nabla \mathbf{u}. \quad (63)$$

$\eta$  is the shear viscosity and  $\zeta$  the volume viscosity. The full stress tensor  $\sigma_{ij} = -p\delta_{ij} + \sigma'_{ij}$  includes the pressure. With this form of the stress tensor  $\sigma'_{ij}$  Eq. (57) is the so-called *Navier–Stokes equation*.

For excitation frequencies far below that of sound waves most of the fluids behave essentially as incompressible fluids

$$\nabla \cdot \mathbf{u}(\mathbf{r}, t) = 0. \quad (\text{condition for incompressibility}) \quad (64)$$

In this case the equation for the momentum density simplifies to

$$\rho \left( \frac{\partial u_i}{\partial t} + u_j \partial_j u_i \right) = -\partial_i p + \partial_j \sigma'_{ij} + \rho f_i \quad (65)$$

and the stress tensor is given by

$$\sigma'_{ij} = \eta \dot{\gamma}_{ij}, \quad (66)$$

with the rate-of-strain tensor

$$\dot{\gamma}_{ij} = \partial_i u_j + \partial_j u_i. \quad (67)$$

In vectorial notation the Eqs. (65) take the form

$$\rho \partial_t \mathbf{u} + \rho (\mathbf{u} \cdot \nabla) \mathbf{u} = -\nabla p + \rho \mathbf{g} + \eta \nabla^2 \mathbf{u}, \quad (68)$$

$\mathbf{g}$  being the gravitational field.

Symmetry considerations, the laws of thermodynamics and an expansion of the transport laws lead to this form of the equations of motion for simple fluids with three positive phenomenological parameters,  $\eta$ ,  $\zeta$  and  $\kappa$ , that may be measured for each fluid. There are three further parameters in the thermodynamic equations of state relating  $T$  with  $\varepsilon$  and  $\rho$  with  $p$ .

For the so-called Boussinesq-approximation the material parameters are assumed to be independent of the temperature, only in front of the gravitational field the variation of the density  $\rho$  with the temperature is taken into account.

$$\rho = \rho_0 \left[ 1 - \alpha(T - T_0) + O((T - T_0)^2) \right] \quad (69)$$

Here  $\alpha$  is the thermal expansion coefficient and  $T_0$  the mean temperature of the fluid layer. Energy conservation and the second law of thermodynamics and the Boussinesq-approximation give the equation for the temperature distribution [1]

$$\partial_t T + (\mathbf{v} \cdot \nabla) T = \kappa \Delta T \quad (70)$$

with the thermal diffusivity  $\kappa$ .

Here we restrict our consideration to two spatial dimensions.  $z$  is the vertical and  $x$  the horizontal coordinate and the  $y$ -coordinate we discard here for reasons of simplicity. In two spatial dimensions the velocity may be expressed by the curl of the velocity potential  $\Psi$ :

$$u_x = \partial_z \Psi, \quad (71)$$

$$u_z = -\partial_x \Psi. \quad (72)$$

With a few straight forward manipulations the Navier-Stokes equations take in two dimension the following form:

$$\partial_t \Delta \Psi + (\partial_z \Psi \partial_x - \partial_x \Psi \partial_z) \Delta \Psi = -g \alpha \partial_x T + \nu \Delta^2 \Psi, \quad (73)$$

$\nu = \frac{\eta}{\rho_0}$  is the kinematic viscosity. The heat transport equation in terms of the potential  $\Psi$  is

$$\partial_t T + (\partial_z \Psi \partial_x - \partial_x \Psi \partial_z) T = \kappa \Delta T. \quad (74)$$

With the height  $d$  of the fluid layer we introduce also dimensionless units

length	$\mathbf{x} = \mathbf{x}' \cdot d$
velocity	$\mathbf{u} = \mathbf{u}' \cdot \frac{\kappa}{d}$
pressure	$\rho = \rho' \cdot \frac{\rho \kappa^2}{d^2}$
temperature	$T = T' \cdot \frac{\kappa \nu}{\alpha g d^3}$
time	$t = t' \cdot \frac{d^2}{\kappa}$

The equations of motion include the dimensionless Prandtl number  $P$

$$P = \frac{\nu}{\kappa} \quad (75)$$

and the dimensionless Rayleigh number

$$R = T_u - T_o = \frac{\alpha g d^3}{\kappa \nu} \Delta T. \quad (76)$$

The rescaled equations include with the Prandtl number only one material constant. For water the Prandtl number is  $P = 7$  and for olive oil one has  $P \approx 950$ . The Rayleigh number is the control parameter of the system. For the remaining part of this appendix all calculations are done in rescaled units but for reasons of simplicity we discard the primes, i.e. for comparison with experimental data the results have to be transformed to the real variables. The rescaled equations of motion are

$$\partial_t \Delta \Psi + (\partial_z \Psi \partial_x - \partial_x \Psi \partial_z) \Delta \Psi = -P \partial_x T + P \Delta^2 \Psi \quad (77)$$

$$\partial_t T + (\partial_z \Psi \partial_x - \partial_x \Psi \partial_z) T = \Delta T. \quad (78)$$

For values of the Prandtl number such as for olive oil in the equations of motion one may choose the limit  $P \rightarrow \infty$ , i.e. in this case the left part of Eq. (77) may be neglected. In this limit the two equations of motion are

$$\Delta^2 \Psi = \partial_x T \quad (79)$$

and

$$\partial_t T + (\partial_z \Psi \partial_x - \partial_x \Psi \partial_z) T = \Delta T. \quad (80)$$

For small temperature differences we expect a linear temperature profile and this may be separated as in the following expression

$$T(t, x, z) = -Rz + T_u + \Theta(t, x, z). \quad (81)$$

With this modification the equations of motion are

$$\partial_t \Delta \Psi + (\partial_z \Psi \partial_x - \partial_x \Psi \partial_z) \Delta \Psi = -P \partial_x \Theta + P \Delta^2 \Psi \quad (82)$$

$$\partial_t \Theta + (\partial_z \Psi \partial_x - \partial_x \Psi \partial_z) \Theta = \Delta \Theta - R \partial_x \Psi. \quad (83)$$

**Boundary conditions.** Fluid motion takes always place in finite systems with boundaries and therefore the boundary conditions for both fields must be specified. We assume that the top and bottom plate are parallel to the  $x - y$  plane and located in scaled units at  $z = 1$  and  $z = 0$ . The temperature at the top plate is denoted with  $T_1$  and at the bottom plate with  $T_2$ . At the boundaries we also assume ideal heat conductivity. In this case boundary condition for the temperature field are

$$T(x, z) = T_1 \quad \text{at} \quad z = 1 \quad \text{and} \quad T(x, z) = T_2 \quad \text{at} \quad z = 0. \quad (84)$$

The component of the velocity that is vertical to the boundary has to vanish at the boundary. This is expressed by

$$v_z(x, z) = 0 \Rightarrow \partial_x \Psi(x, z) = 0 \quad \text{at} \quad z = 0, 1. \quad (85)$$

The motion of the fluid parallel to the boundaries vanishes at the boundaries due to viscous friction:

$$v_x(x, z) = 0 \Rightarrow \partial_z \Psi(x, z) = 0 \quad \text{at} \quad z = 0, 1. \quad (86)$$

Velocity boundary conditions of this type are called *rigid boundary conditions*. For analytical calculations often *free slip* boundary conditions are more appropriate. In this case the velocity parallel to the boundaries does not experience friction. I.e. there are no shear forces at boundaries and the non diagonal elements of the stress tensor

$$\sigma_{xz} = \eta(\partial_z v_x + \partial_x v_z)$$

vanish. If the continuity equation is taken into account one obtains the following boundary condition for the velocity potential

$$\partial_z^2 \Psi(x, z) = 0 \quad \text{at} \quad z = 0, 1. \quad (87)$$

For the velocity potential one has the freedom to choose an additive constant such, that the velocity potential vanishes at the boundary.

## B Derivation of the Oseen–Tensor

In this section we derive in the limit of a the Reynolds–number  $Re \ll 1$  from Stokes equation (17),

$$\eta \Delta \mathbf{u}' - \nabla p' + \mathbf{f} = 0, \quad (88)$$

the Oseen–Tensor, describing the hydrodynamic interaction of moving particles. This is a linear partial differential equation and may be solved by Fourier-transformation of  $\mathbf{u}'(\mathbf{r}, t)$ ,  $p'(\mathbf{r}, t)$  and  $\mathbf{f}(\mathbf{r}, t)$ :

$$\begin{aligned}\mathbf{u}'(\mathbf{r}) &= \int \frac{d^3\mathbf{k}}{(2\pi)^3} \mathbf{u}'(\mathbf{k}) e^{i\mathbf{k}\cdot\mathbf{r}}, \\ p'(\mathbf{r}) &= \int \frac{d^3\mathbf{k}}{(2\pi)^3} p'(\mathbf{k}) e^{i\mathbf{k}\cdot\mathbf{r}}, \\ \mathbf{f}(\mathbf{r}) &= \int \frac{d^3\mathbf{k}}{(2\pi)^3} \mathbf{f}(\mathbf{k}) e^{i\mathbf{k}\cdot\mathbf{r}}.\end{aligned}\quad (89)$$

With this ansatz the linear Stokes equation (88) and the incompressibility condition take the form

$$\begin{aligned}\eta \mathbf{k}^2 \mathbf{u}'(\mathbf{k}) + i\mathbf{k} p'(\mathbf{k}) &= \mathbf{f}(\mathbf{k}), \\ \mathbf{k} \cdot \mathbf{u}'(\mathbf{k}) &= 0.\end{aligned}\quad (90)$$

Multiplication of equation (88) with wave number  $\mathbf{k}$  leads to

$$\begin{aligned}\underbrace{-i\eta \mathbf{k}^2 \mathbf{k} \cdot \mathbf{u}'(\mathbf{k})}_{\equiv 0} + \mathbf{k} \cdot \mathbf{k} p'(\mathbf{k}) &= -i\mathbf{k} \cdot \mathbf{f}(\mathbf{k}) \\ \rightarrow p'(\mathbf{k}) &= -i \frac{\mathbf{k} \cdot \mathbf{f}}{\mathbf{k}^2}.\end{aligned}\quad (91)$$

and this gives together with (90)

$$\mathbf{u}'(\mathbf{k}) = \frac{1}{\eta \mathbf{k}^2} \left( \mathbf{1} - \hat{\mathbf{k}}\hat{\mathbf{k}} \right) \cdot \mathbf{f}(\mathbf{k}), \quad (92)$$

for the perturbed velocity field  $\mathbf{u}'$  as function of the force field  $\mathbf{f}$  ( $\hat{\mathbf{k}}\hat{\mathbf{k}}$  describes a dyadic product). In real space one has a *nonlocal* relation between the flow perturbation and the force field

$$\begin{aligned}\mathbf{u}'(\mathbf{r}) &= \int \frac{d^3\mathbf{k}}{(2\pi)^3} \frac{1}{\eta \mathbf{k}^2} \left( \mathbf{1} - \hat{\mathbf{k}}\hat{\mathbf{k}} \right) \cdot \mathbf{f}(\mathbf{k}) \\ &= \int d^3\mathbf{r} \left\{ \int \frac{d^3\mathbf{k}}{(2\pi)^3} \frac{1}{\eta \mathbf{k}^2} \left( \mathbf{1} - \hat{\mathbf{k}}\hat{\mathbf{k}} \right) e^{i\mathbf{k}\cdot(\mathbf{r}-\mathbf{r})} \right\} \cdot \mathbf{f}(\mathbf{r}) \\ &= \int d^3\mathbf{r} \Omega(\mathbf{r} - \mathbf{r}) \cdot \mathbf{f}(\mathbf{r}),\end{aligned}\quad (93)$$

with unit matrix  $\mathbf{1}$  and the explicit form of the integral kernel

$$\Omega(\mathbf{r}) = \int \frac{d^3\mathbf{k}}{(2\pi)^3} \frac{1}{\eta \mathbf{k}^2} \left( \mathbf{1} - \hat{\mathbf{k}}\hat{\mathbf{k}} \right) e^{i\mathbf{k}\cdot\mathbf{r}}. \quad (94)$$

The relation between  $\mathbf{u}'$  and  $\mathbf{f}$  is nonlocal but linear. For the evaluation of the integral we use the isotropy of space and therefore the ansatz

$$\Omega_{\alpha\beta} = A\delta_{\alpha\beta} + B\hat{r}_\alpha\hat{r}_\beta. \quad (95)$$

The trace of the matrix  $\Omega$  is

$$\begin{aligned} Tr(\Omega) &\equiv \Omega_{\alpha\alpha} = 3A + B = \frac{1}{(2\pi)^3} \int d^3\mathbf{k} \frac{1}{\eta k^2} (3-1) e^{i\mathbf{k}\cdot\mathbf{r}} \\ &= \frac{1}{(2\pi)^3} \frac{8\pi}{\eta r} \underbrace{\int_0^\infty dk \frac{\sin(kr)}{k}}_{\pi/2} = \frac{1}{2\pi\eta r} . \end{aligned} \quad (96)$$

With tensor contraction of  $\Omega$

$$\begin{aligned} \hat{\mathbf{r}} \cdot \Omega \cdot \hat{\mathbf{r}} &= \hat{r}_\alpha \Omega_{\alpha\beta} \hat{r}_\beta \\ &= A \hat{r}_\alpha \delta_{\alpha\beta} \hat{r}_\beta + B \hat{r}_\alpha (\hat{r}_\alpha \hat{r}_\beta) \hat{r}_\beta \\ &= A + B = \int \frac{d^3\mathbf{k}}{(2\pi)^3} \frac{1}{\eta k^2} \left[ 1 - (\hat{\mathbf{k}} \cdot \hat{\mathbf{r}})^2 \right] e^{i\mathbf{k}\cdot\mathbf{r}} \\ &= \frac{1}{(2\pi)^2 \eta} \int_0^\infty \int_0^\pi dk d\cos\theta (1 - \cos^2\theta) e^{ikr \cos\theta} \\ &= \frac{1}{(2\pi)^2 \eta} \left\{ \int_0^\infty dk \frac{2 \sin kr}{r k} \right. \\ &\quad \left. - \int_0^\infty dk d\cos\theta \frac{1}{(ir)^2} \partial_k^2 e^{ikr \cos\theta} \right\} \\ &= \frac{1}{(2\pi)^2 \eta} \left\{ \frac{\pi}{r} + \frac{2i}{r^3} \partial_k \left( \frac{\sin kr}{k} \right)_0^\infty \right\} \\ &\stackrel{\text{L'Hospital}}{=} \frac{1}{4\pi\eta r} + \frac{2i}{(2\pi)^2 \eta r} \underbrace{\left( \frac{-kr^2 \sin kr}{2k} \right)}_{\substack{k \rightarrow 0 \\ \rightarrow 0}} \\ &= \frac{1}{4\pi\eta r} . \end{aligned} \quad (97)$$

one obtains a second equation for the determination of the two constants  $A$  and  $B$ :

$$\left. \begin{aligned} 3A + B &= \frac{1}{2\pi\eta r} \\ A + B &= \frac{1}{4\pi\eta r} \end{aligned} \right\} \implies A = B = \frac{1}{8\pi\eta r} ,$$

The final form of the matrix

$$\Omega(\mathbf{r}) = \frac{1}{8\pi\eta r} (\mathbf{1} + \hat{\mathbf{r}}\hat{\mathbf{r}}) . \quad (98)$$

is the so-called Oseen–Tensor.

## References

- [1] L. D. Landau, E. M. Lifshitz, *Course in Theoretical Physics: Fluid Dynamics*, Butterworth, Boston, 1987.
- [2] D. J. Acheson, *Elementary Fluid Dynamics*, Oxford, Oxford, 1990.
- [3] B. Hof et al. *Experimental observation of nonlinear traveling waves in turbulent pipe flow*, Science 205 (2004) 1594.



- [4] F. H. Busse, Visualizing the dynamics of the onset of turbulence, *Science* 305 (2004) 1574.
- [5] G. Ahlers, S. Grossmann, D. Lohse, Hochpräzision in Kochtopf, *Physik J. 2* (2002) 31.
- [6] F. H. Busse, *The sequence-of-Bifurcations approach towards understanding turbulent fluid flow*, *Surveys in Geophysics* **24** (2003) 269.
- [7] A. Buka, L. Kramer, *Pattern Formation in Liquid Crystals*, Springer, Berlin, 1996.
- [8] L. Kramer, W. Pesch, Convection instabilities in nematic liquid crystals, *Annu. Rev. Fluid Mech.* 27 (1995) 515.
- [9] E. N. Lorenz, *J. Atmos. Sci.* 20 (1963) 130.
- [10] J. Stavans, F. Heslot, A. Libchaber, Fixed winding number and the quasiperiodic route to chaos in a convective fluid, *Phys. Rev. Lett.* 55 (1985) 596.
- [11] E. Bodenschatz, W. Pesch, G. Ahlers, Recent developments in Rayleigh-Génard convection, *Annu. Rev. Fluid Mech.* 32 (2000) 709.
- [12] M. C. Cross, P. C. Hohenberg, Pattern formation outside of equilibrium, *Rev. Mod. Phys.* 65 (1993) 851.
- [13] P. Tabeling, *Introduction of Microfluidics*, Oxford Univ. Press, Oxford, 2006.
- [14] W. Zimmermann, Pattern formation in electrohydrodynamic convection, *Mat. Res. Bulletin* 16 (1991) 46.
- [15] S. Kai, W. Zimmermann, M. Andoh, N. Chizumi, Spontaneous nucleation of turbulence in the electrohydrodynamics and its similarity with crystal growth, *Jap. Jour. Phys. Soc.* 58 (1989) 3449.
- [16] S. Nasuno, O. Sasaki, S. Kai, W. Zimmermann, Secondary instabilities in electrohydrodynamic convection of nematics, *Phys. Rev. A* 46 (1992) 4954.
- [17] F. H. Busse, S. C. Müller (Eds.), *Evolution of Spontaneous Structures in Dissipative Continuous Systems*, Springer, Berlin, 1998.
- [18] B. Dressel, A. Joets, L. Pastur, W. Pesch, E. Plaut, R. Ribotta, Complex spatio-temporal convection patterns, *PRL* 88 (2002) 024503.
- [19] A. Einstein, Eine neue Bestimmung der Moleküldimension, *Ann. Phys.* 19 (1906) 289.
- [20] C. Misbah, Vacillating Breathing and Tumbling of Vesicles under Shear Flow, *Phys. Rev. Lett.* 96 (2006) 028104.
- [21] R. G. Larson, *The Structure and Rheology of Complex Fluids*, Oxford Press, Oxford, 1999.
- [22] R. E. Rosenzweig, *Ferrohydrodynamics* (Cambridge University Press, Cambridge, 1985).
- [23] S. Odenbach, Ferrofluide - ihre Grundlagen und Anwendungen, *Physik in unserer Zeit* 32 (2001) 122.

- [24] T. C. Halsey, *Science* **258**, 761 (1992); T. C. Halsey and J. E. Martin, *Scientific American* **58** Oct. 1993.
- [25] M. Kraus, W. Wintz, U. Seifert and R. Lipowsky, *Phys. Rev. Lett.* **77**, 3685 (1996); M. Abkarian, C. Lartigue and A. Viallat, *Phys. Rev. Lett.* **88**, 068103 (2002) and references therein.
- [26] R. Bird, C. Curtiss, R. Armstrong, O. Hassager, *Dynamics of Polymeric Liquids I, II*, Wiley & Sons, New York, 1987.
- [27] J. F. Brady and G. Bossis, *Stokesian Dynamics*, *Ann. Rev. Fluid Mech.* **20**, 111 (1988); D.R. Foss and J. F. Brady, *Structure, diffusion and rheology of Brownian suspensions by Stokesian Dynamics simulation*, *J. Fluid. Mech.* **407**, 167 (2000);
- [28] A. Arendt, J. Leonhard, D. Kienle, G. Ristow, R. Rzehak and W. Zimmermann, *Cross-Streamline migration of deformable objects in Poiseuille flow* (to be published).
- [29] A. Groisman, V. Steinberg, Elastic turbulence in a polymer solution flow, *Nature* **405** (2000) 53.
- [30] A. Groisman, V. Steinberg, Stretching of polymers in a random three-dimensional flow, *Phys. Rev. Lett.* **86** (2001) 934.
- [31] P. M. Chaikin, T. C. Lubensky, *Principles of condensed matter physics*, Cambridge Univ. Press, Cambridge, UK, 1995.
- [32] D. J. Tritton, *Physical Fluid Dynamics*, Clarendon Press, Oxford, 1987.
- [33] H. Bénard, *Gén. Sci. Pures Appl.* **11** (1900) 1261 and 1309.
- [34] H. Bénard, Les tourbillons cellulaires dans une nappe liquide transportent de la chaleur par convection en regime permanent, *Ann. Chim. Phys.* **23** (1902) 62.
- [35] S. Chandrasekhar, *Hydrodynamic and Hydromagnetic Stability*, Oxford University Press, London, 1961.
- [36] F. H. Busse, Nonlinear properties of convection, *Rep. Prog. Phys.* **41** (1978) 1929.
- [37] F. H. Busse, Transition to turbulence in Rayleigh–Bénard convection, in: H. L. Swinney, J. P. Gollub (Eds.), *Hydrodynamic Instabilities and the Transition to Turbulence*, Vol. 45 of *Topic in Applied Physics*, Springer, New York, 1986.
- [38] L. Rayleigh, On the dynamics of evolving fluids, *Proc. R. Soc. London. Ser. A* **93** (1916) 148.
- [39] L. Rayleigh, *Phil. Mag.* **32** (1916) 529.
- [40] P. Manneville, *Dissipative Structures and Weak Turbulence*, Academic Press, London, 1990.
- [41] W. Schöpf, W. Zimmermann, Convection in binary fluids: Amplitude equations, codimension-2 bifurcation, and thermal fluctuations, *Phys. Rev. E* **47** (1993) 1739.

- [42] A. C. Newell, J. A. Whitehead, Finite bandwidth finite amplitude convection, *J. Fluid Mech.* **38** (1969) 279.
- [43] W. Zimmermann, Elementare Konzepte der Strukturbildung, in: K. Kehr, H. Müller-Krumbhaar (Eds.), *Dynamik und Strukturbildung in kondensierter Materie*, FZ Jülich, Jülich, 1997.
- [44] H. Tennekes, J. L. Lumely, *A First Course in Turbulence*, MIT Press, Cambridge Mass, 1972.
- [45] S. B. Pope, *Turbulent Flows*, Cambridge Univ. Press, Cambridge, 2000.
- [46] R. Krishnamurty and L. N. Howard, *Proc. Nat. Acad. Sci.* **78**, 1981 (1981).
- [47] R. E. Kelly and D. Pal, *Thermal convection with spatially periodic boundary conditions; resonant wavelength excitation*, *J. Fluid Mech.* **86** (1978) 433; G. Hartung, F. H. Busse and I. Rehberg, *Time-Dependent Convection Induced by Broken Spatial Symmetries*, *Phys. Rev. Lett.* **66** (1991) 2741; W. Zimmermann and R. Schmitz, *Hopf bifurcation by frustrated drifts*, *Phys. Rev. E* **53** (1996) R1321; R. Schmitz and W. Zimmermann, *Spatially periodic modulated Rayleigh-Bénard convection*, *Phys. Rev. E* **53** (1996) 5993; R. Schmitz and W. Zimmermann, *Orientational oscillations of stripe patterns induced by frustrated drifts*, *Phys. Lett. A* **231** (1997) 185; W. Zimmermann, B. Painter and R. Behringer, *Pattern Formation in inhomogeneous convective systems*, *Eur. Phys. J. B* **5** (1998) 575.
- [48] R. Rzehak, D. Kienle, T. Kawakatsu, and W. Zimmermann, *Partial draining of a tethered polymer in flow*, *Europhys. Lett.* **26**, 821 (1999); R. Rzehak, W. Kromen, T. Kawakatsu, W. Zimmermann, *Deformations of tethered polymers in uniform flow*, *Euro. Phys. J. E* **2** (2000) 3; D. Kienle and W. Zimmermann, *F-shell Blob Model for a Tethered Polymer in Strong Flows*, *Macromolecules* **34**, 9173 (2001); R. Rzehak and W. Zimmermann, *On the Dynamics of tethered Polymers in strong flows*, *Europhys. Lett.* **59** 779 (2002); R. Rzehak and W. Zimmermann, *Static Dynamics Approach to Relaxation Modes and -Times for Nonlinear Polymer Models*, *Phys. Rev. E* **68** (2003) 021804.
- [49] G. K. Batchelor, J. T. Green, The determination of the bulk stress in a suspension of spherical particles to order  $c^2$ , *J. Fluid Mech.* **56** (1972) 401.
- [50] A. Groisman, V. Steinberg, Elastic turbulence in curvilinear flows of polymer solutions, *New Journal of Physics* **6** (2004) 29.
- [51] D. E. Smith, H. P. Babcock, S. Chu, Single-polymer dynamics in steady shear flow, *Science* **283** (1999) 1724.
- [52] A. Groisman, V. Steinberg, Elastic turbulence in a polymer solution flow, *Nature* **405** (2000) 53.
- [53] A. Groisman, V. Steinberg, Efficient mixing at low Reynolds numbers using polymer additives, *Nature* **405** (2001) 410.
- [54] L. D. Landau, E. M. Lifshitz, *LEHRBUCH DER THEORETISCHEN PHYSIK VII: Elastizitätstheorie*, Akademie Verlag, Berlin, 1990.

- [55] P. G. de Gennes, J. Prost, *The Physics of Liquid Crystals*, Clarendon, Oxford, 1993.
- [56] H. Temmen, H. Pleiner, M. Liu, H. R. Brand, Convective Nonlinearity in Non-Newtonian Fluids, *Phys. Rev. Lett.* 84 (2000) 3228.